



Complex Organic Molecules in Star-Forming Regions of the Magellanic Clouds

Downloaded from: <https://research.chalmers.se>, 2025-12-05 01:47 UTC

Citation for the original published paper (version of record):

Sewiło, M., Charnley, S., Schilke, P. et al (2019). Complex Organic Molecules in Star-Forming Regions of the Magellanic Clouds. *ACS Earth and Space Chemistry*, 3(10): 2088-2109.
<http://dx.doi.org/10.1021/acsearthspacechem.9b00065>

N.B. When citing this work, cite the original published paper.

Complex Organic Molecules in Star-Forming Regions of the Magellanic Clouds

Marta Sewilo,^{*,†,‡,§} Steven B. Charnley,[¶] Peter Schilke,[§] Vianney Taquet,^{||} Joana M. Oliveira,[⊥] Takashi Shimonishi,^{#,×} Eva Wiström,[▽] Remy Indebetouw,^{◇,◆} Jacob L. Ward,[⊗] Jacco Th. van Loon,^{⊥,Ⓛ} Jennifer Wiseman,[○] Sarolta Zahorecz,^{■,☆} Toshikazu Onishi,[■] Akiko Kawamura,[@] C.-H. Rosie Chen,[▲] Yasuo Fukui,[□] and Roya Hamedani Golshan[§]

[†]CRESST II and Exoplanets and Stellar Astrophysics Laboratory, NASA Goddard Space Flight Center, Greenbelt, Maryland 20771, United States

[‡]Department of Astronomy, University of Maryland, College Park, Maryland 20742, United States

[¶]Astrochemistry Laboratory, NASA Goddard Space Flight Center, Greenbelt, Maryland 20771, United States

[§]I. Physikalisches Institut der Universität zu Köln, D-50937 Köln, Germany

^{||}Osservatorio Astrofisico di Arcetri, Istituto Nazionale di Astrofisica (INAF), 50125 Firenze, Italy

[⊥]Lennard-Jones Laboratories, Keele University, Newcastle ST5 5BG, U.K.

[#]Frontier Research Institute for Interdisciplinary Sciences, Tohoku University, Sendai, Miyaga 9980-8578, Japan

[×]Astronomical Institute, Tohoku University, Sendai, Miyaga 9980-8578, Japan

[▽]Onsala Space Observatory, Department of Space, Earth and Environment, Chalmers University of Technology, 43992 Onsala, Sweden

[◇]Department of Astronomy, University of Virginia, Charlottesville, Virginia 22904, United States

[◆]National Radio Astronomy Observatory, Charlottesville, Virginia 22903, United States

[⊗]Astronomisches Rechen-Institut, Zentrum für Astronomie der Universität Heidelberg, D-69120 Heidelberg, Germany

[○]NASA Goddard Space Flight Center, Greenbelt, Maryland 20771, United States

[■]Department of Physical Science, Graduate School of Science, Osaka Prefecture University, Sakai, Osaka 599-8531, Japan

[☆]Chile Observatory, National Astronomical Observatory of Japan, National Institutes of Natural Sciences, Mitaka, Tokyo 181-8588, Japan

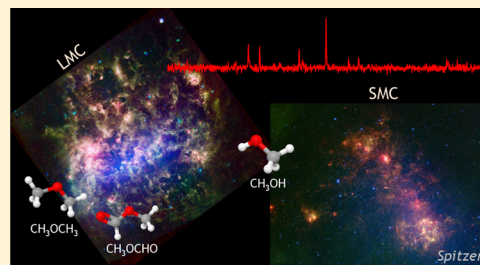
[@]National Astronomical Observatory of Japan, Mitaka, Tokyo 181-8588, Japan

[▲]Max-Planck-Institut für Radioastronomie, D-53121 Bonn, Germany

[□]School of Science, Nagoya University, Chikusa-ku, Nagoya 464-8602, Japan

ABSTRACT: The Large and Small Magellanic Clouds (LMC and SMC), gas-rich dwarf companions of the Milky Way, are the nearest laboratories for detailed studies on the formation and survival of complex organic molecules (COMs) under metal-poor conditions. To date, only methanol, methyl formate, and dimethyl ether have been detected in these galaxies—all three toward two hot cores in the N113 star-forming region in the LMC, the only extragalactic sources exhibiting complex hot-core chemistry. We describe a small and diverse sample of the LMC and SMC sources associated with COMs or hot-core chemistry, and compare the observations to theoretical model predictions. Theoretical models accounting for the physical conditions and metallicity of hot molecular cores in the Magellanic Clouds have been able to broadly account for the existing observations, but they fail to reproduce the dimethyl ether abundance by more than an order of magnitude. We discuss future prospects for research in the field of complex chemistry in the low-metallicity environment. The detection of COMs in the Magellanic Clouds has important implications for astrobiology. The metallicity of the Magellanic Clouds is similar to that of galaxies in the earlier epochs of the universe; thus, the presence of COMs in the LMC and SMC indicates that a similar prebiotic chemistry leading to the emergence of life, as it happened on Earth, is possible in low-metallicity systems in the earlier universe.

KEYWORDS: *Magellanic Clouds, star formation, astrochemistry, complex organic molecules, molecular abundances*



1. INTRODUCTION

An important issue for astrochemistry is to understand how the organic chemistry in low-metallicity environments (i.e., with low abundances of elements heavier than hydrogen or helium), relevant for star formation at earlier epochs of cosmic evolution, differs from that in the Galaxy. Large aromatic organic molecules

Special Issue: Complex Organic Molecules (COMs) in Star-Forming Regions

Received: March 19, 2019

Revised: August 26, 2019

Accepted: August 27, 2019

Published: August 27, 2019

such as polycyclic aromatic hydrocarbons (PAHs) are detected in high-redshift galaxies, but the formation efficiency of smaller complex organic molecules (COMs) has been unknown. A quantitative determination of the organic chemistry in high-redshift galaxies with different star formation histories, and lower abundances of the important biogenic elements (C, O, N, S, P), can shed light on the inventory of COMs available to planetary systems and their potential for harboring life (e.g., ref 1). The nearest laboratories for detailed studies of star formation under metal-poor conditions are the Large and Small Magellanic Clouds (LMC and SMC).

The LMC and SMC are gas-rich dwarf companions of the Milky Way located at a distance of (50.0 ± 1.1) kpc (ref 2) and (62.1 ± 2.0) kpc (ref 3), respectively. They are the nearest star-forming galaxies with metallicities Z (the mass fractions of all the chemical elements other than hydrogen and helium) lower than that in the solar neighborhood ($Z_{\odot} = 0.0134$):⁴ $Z_{\text{LMC}} \approx 0.3\text{--}0.5 Z_{\odot}$ and $Z_{\text{SMC}} \approx 0.2 Z_{\odot}$.^{5,6} Apart from the lower elemental abundances of gaseous C, O, and N atoms (e.g., ref 7), low metallicity leads to less shielding (due to the lower dust abundance; e.g., refs 8 and 9), greater penetration of UV photons into the interstellar medium, and consequently warmer dust grains (e.g., refs 10 and 11). The interstellar ultraviolet radiation field in the LMC and SMC is 10–100 higher than typical Galactic values (e.g., ref 12). Gamma-ray observations indicate that the cosmic-ray density in the LMC and SMC is respectively $\sim 25\%$ and $\sim 15\%$ of that measured in the solar neighborhood (refs 13 and 14). All these low-metallicity effects may have direct consequences on the formation efficiency and survival of COMs, although their relative importance remains unclear.

The range of metallicities observed in the Magellanic Clouds is similar to that in galaxies at redshift $z \approx 1.5\text{--}2$, i.e., at the peak of the star formation in the universe (between ~ 2.8 and ~ 3.5 billion years after the Big Bang; e.g., ref 15), making them ideal templates for studying star formation and complex chemistry in low-metallicity systems in an earlier universe where direct measurements of resolved stellar populations are not possible. Only very recently have gaseous COMs (methanol: CH_3OH , methyl formate: HCOOCH_3 , dimethyl ether: CH_3OCH_3) been detected in the LMC^{16–18} and in the SMC,¹⁹ using the Atacama Large Millimeter/sub-millimeter Array (ALMA). These observations showed that interstellar COMs can form in the low-metallicity environments, probably in the hot molecular cores and corinos associated with massive and low- to intermediate-mass protostars, respectively. COMs had previously been detected outside the Milky Way, but in galaxies with metallicities comparable to or higher than solar values (see ref 20 and references therein).

In this Review, we summarize the current state of knowledge concerning the organic chemistry in the Magellanic Clouds.

2. MOLECULAR LINE INVENTORIES IN STAR-FORMING REGIONS OF THE MAGELLANIC CLOUDS

The proximity of the LMC/SMC enables both detailed studies of individual star-forming regions and statistical studies of molecular clouds or stellar populations on galactic scales. The systematic studies of molecular clouds in the Magellanic Clouds started with the $^{12}\text{CO } J = 1\text{--}0$ survey of the LMC (central $6^\circ \times 6^\circ$)²² and the SMC ($2^\circ \times 2^\circ$),²³ with a resolution of $8''.8$ (the Columbia 1.2-m Millimeter-Wave Telescope), followed by a higher resolution ($2''.6$) survey of both galaxies with the

NANTEN 4-m telescope (e.g., refs 24 and 25). The more sensitive NANTEN survey that identified 272 molecular clouds in the LMC was published in ref 26. The most luminous CO clouds from this survey were observed with $45''$ resolution using the Australia Telescope National Facility (ATNF) Mopra 22-m Telescope (the MAGMA survey).²⁷

The molecular gas in the Magellanic Clouds was also investigated using the CO data from the ESO SEST (Swedish/ESO Submillimeter Telescope) Key-Program (CO $J = 1\text{--}0$ and $2\text{--}1$ lines with $50''$ and $25''$ half-power beam widths, HPBW) toward 92 and 42 positions in the LMC and SMC, respectively, mostly coincident with IRAS sources; the results were reported in multiple papers, including detailed studies of major star-forming giant molecular clouds (GMCs) and less active cloud complexes in the LMC and small molecular cloud complexes in the SMC (see ref 29 and references therein). Many other CO studies of individual star-forming regions with SEST in both the LMC and SMC followed (e.g., LMC regions N159W, N113, N44BC, and N214DE).³⁰

The first unbiased spectral line survey of an individual star-forming region in the LMC was reported in ref 31, using SEST and centered on the N159W molecular peak in N159—the brightest NANTEN GMC with H II regions. The observations covered a 215–245 GHz frequency range in several bands and selected bright lines at lower frequencies (~ 100 GHz; HPBW $\sim 23''$ at 220 GHz and $50''$ at 100 GHz). No COM transitions covered by these observations (e.g., propyne: $\text{CH}_3\text{CCH } J = 5\text{--}4$ and $J = 6\text{--}5$ and $\text{CH}_3\text{OCH}_3 J = 6\text{--}5$ lines) were detected. In ref 31, it was reported that fractional abundances with respect to H_2 for molecules detected in N159W (^{13}CO , C^{18}O , CS, SO, HCO^+ , HCN, HNC, CN, and H_2CO (formaldehyde)) are typically a factor of 10 lower than those observed in the Galaxy.

The multi-region, multi-line SEST 3 mm (85–115 GHz) survey described in ref 32 focused on one SMC (LIRS 36 or N12) and four LMC (N113, N44BC, N159HW, and N214DE) molecular cloud cores. They detected the C_2H , HCN, HCO^+ , HNC, CS, ^{13}CO , CN, and ^{12}CO transitions, but the $\text{CH}_3\text{OH } J = 2\text{--}1$ line at ~ 96.74 GHz covered by their observations was not detected toward any of the regions. The follow-up study on N12 in the SMC included the 2, 1.3, and 0.85 mm SEST bands, but also failed to detect CH_3OH or other COMs.³³

The first detection of a COM in the Magellanic Clouds was reported in ref 16 for a SEST 0.85, 1.3, 2, and 3 mm survey of the SMC LIRS 49 (or N27) and LMC 30 Dor-10, 30 Dor-27, N159W, N159S, and N160 regions, covering a range of metallicities and UV radiation strengths. N159W was the only region where CH_3OH was detected: $J = 2\text{--}1$ and two $3\text{--}2$ lines at ~ 96.7 and ~ 145.1 GHz, respectively (see Table 1). The observations in ref 16 covered the $J = 6\text{--}5$ and $J = 8\text{--}7$ lines of CH_3CCH , but only marginal ($\sim 2.5\sigma$) detections are reported toward one region: N159W. The CH_3OH fractional abundance with respect to H_2 was estimated to be 4.3×10^{-10} in N159W. The authors indicated that the derived physical and chemical quantities are averages over spatial scales probed by their observations (10–15 pc in the 3 mm, and 5–10 pc in the 2/1.3 mm bands). Overall, the molecular abundances in N159W where CH_3OH was detected are typically 5–20 times lower than those measured in the Galactic molecular clouds, assuming that hydrogen is mainly in molecular form within the clouds. It was concluded that reduced abundances are likely to be a combined effect of lower abundances of carbon and oxygen and higher photodissociation rates of molecules, both due to the lower metallicity in the LMC.

Table 1. CH₃OH Transitions Detected in the LMC in Single-Dish Observations^{a,b}

region	species	transition	frequency (GHz)	E _u (K)	ref
N159W	CH ₃ OH, $\nu_t = 0^c$	2 _{-1,2} –1 _{-1,1} E	96.739362	12.54	16
		2 _{0,2} –1 _{0,1} A ⁺	96.741375	6.97	16
		2 _{0,2} –1 _{0,1} E	96.744550	20.09	16
		2 _{1,1} –1 _{1,0} E	96.755511	28.01	16
		3 _{-1,3} –2 _{-1,2} E	145.09747	19.51	16
		3 _{0,3} –2 _{0,2} A ⁺	145.10323	13.93	16
N113	CH ₃ OH, $\nu_t = 0$	2 _{-1,2} –1 _{-1,1} E	96.739362	12.54	17
		2 _{0,2} –1 _{0,1} A ⁺	96.741375	6.97	17
		3 _{-1,3} –2 _{-1,2} E	145.09747	19.51	17
		3 _{0,3} –2 _{0,2} A ⁺	145.10323	13.93	17

^aAll the observations were conducted with SEST. The SEST's half-power beam sizes are 61"–54" and 47"–24" in frequency ranges of 85–98 and 109–219 GHz, respectively.¹⁷ ^bThe table uses the Cologne Database for Molecular Spectroscopy (CDMS) notation from the National Radio Astronomy Observatory (NRAO) Spectral Line Catalog (Splatalogue). For CH₃OH ($N K_a K_c p \nu$), a sign value of K_a is used to differentiate E_1 (+) and E_2 (–) states (both belong to the same E symmetry species). ^cThe four transitions at ~96.7 GHz are blended.

An extensive spectral line study on N113, previously observed in ref 32 at 3 mm (see above), provided new detections of CH₃OH.¹⁷ Their SEST observations covered the 0.85, 1.3, 2, and 3 mm bands. The rich spectral line inventory included two $J = 2-1$ and two $J = 3-2$ lines of CH₃OH (see Table 1). The CH₃OH abundance with respect to H₂ was estimated to be $\sim 5 \times 10^{-10}$, similar to that observed in N159W in ref 16, and an order of magnitude lower than that observed in the Galaxy.

N113 and N159W remain the best-studied regions in the LMC in terms of chemical inventory. The initial single-dish surveys were followed by interferometric observations with the Australia Telescope Compact Array (ATCA) with 4"–6" angular resolutions (N113 only, ref 34, and N113, N159, N105, and N44, ref 35) that focused on dense gas tracers such as HCO⁺ and HCN. The authors of ref 36 searched for NH₃ (1, 1) and (2, 2) in seven star-forming regions in the LMC (N113, N159W, N159S, 30 Dor 10, N44 BC, N105 A, and N83 A) with ATCA (HPBW $\approx 9''$ – $17''$) and only detected it toward N159W with an abundance of $\sim 4 \times 10^{-10}$ with respect to H₂: 1.5–5 orders of magnitude lower than observed in Galactic star-forming regions.

The most recent multi-region, multi-line single-dish survey, described in ref 37, used the Mopra 22-m telescope's 3 mm band (HPBW $\approx 38''$ at 90 GHz and $30''$ at 115 GHz). The sample included seven H II regions: NQC2, CO Peak 1, N79, N44C, N11B, N113, and N159W. That work confirmed lower molecular abundances in the LMC star-forming regions. Those observations failed to detect CH₃OH and other COMs.

The results of the single-dish molecular line surveys of individual H II regions in the LMC and SMC indicate a deficiency of CH₃OH in these low-metallicity galaxies. This deficiency is also supported by the low detection rate of CH₃OH masers in the Magellanic Clouds. Ref 38 described a complete systematic survey for 6668 MHz CH₃OH and 6035 MHz excited-state OH masers in both the LMC and SMC using the Methanol Multibeam (MMB) survey receiver on the 64-m Parkes telescope (HPBW $\approx 3.3'$), supplemented by higher sensitivity targeted observations of known star-forming regions. The survey resulted in a detection of only one maser of each kind, increasing the number of known 6668 MHz CH₃OH masers in the LMC to four.^{39–41} Ref 42 later reported detection of a single 12.2 GHz CH₃OH maser in the LMC. To date, no CH₃OH masers have been detected in the SMC. The authors of ref 38 estimated that CH₃OH masers in the LMC are under-

abundant by a factor of ~ 45 (or $\sim 4-5$ after correcting for differences in the star formation rates between the galaxies) and interstellar OH and H₂O masers by a factor of ~ 10 compared to the Galaxy.

The Spitzer Space Telescope (referred to herein simply as *Spitzer*)⁴³ and Herschel Space Observatory (referred to as *Herschel*)⁴⁴ enabled studies of young stellar object (YSO) populations in the LMC and SMC, both galaxy-wide and in individual star-forming regions. Using the data from the *Spitzer* "Surveying the Agents of Galaxy Evolution" (SAGE)⁴⁵ and "Surveying the Agents of Galaxy Evolution in the Tidally Stripped, Low Metallicity Small Magellanic Cloud" (SAGE-SMC),⁴⁶ thousands of YSO candidates were identified in the Magellanic Clouds, dramatically increasing the number of previously known YSOs (from 20/1 in the LMC/SMC; e.g., refs 47–52). YSOs detected by *Spitzer* include mostly Stage I (protostars with accreting envelopes and disks) and also Stage II (disk-only) YSOs; the youngest Stage 0/I YSOs (protostars in the main accretion stage) were identified with *Herschel* using the data from the "HERschel Inventory of The Agents of Galaxy Evolution" (HERITAGE)²¹ survey (e.g., refs 53 and 54). The AKARI "Large-area Survey of the Large Magellanic Cloud" (LSLMC) also carried out near- to mid-infrared photometric survey and near-infrared slitless spectroscopic survey toward the LMC, whose data sets also are used to search for YSOs in the LMC.^{55–57} On a galaxy-wide scale, YSO lists can be utilized to determine a star formation rate in each galaxy. On scales of individual star-forming clouds, YSO catalogs can also be used to study star formation rate, star formation efficiency, and the evolutionary stage of the GMCs and to provide targets for follow-up detailed observations.

Spectroscopic follow-up observations of *Spitzer*, *Herschel*, and AKARI YSO candidates in the LMC and SMC revealed chemical differences in the YSO envelopes between these galaxies and compared to Galactic YSOs, which can be explained as a consequence of differences in metallicity (see section 3).

3. NEAR- TO MID-INFRARED SPECTROSCOPY: MORE EVIDENCE FOR CHEMICAL DIFFERENCES BETWEEN THE LMC, SMC, AND THE MILKY WAY

The mid-infrared studies on the LMC YSOs with *Spitzer* Infrared Spectrograph (IRS)^{11,58–60} and near-infrared studies with the AKARI satellite^{61,62} and ground-based instrumentation^{11,59} found differences in ice chemistry between the LMC

and the Galaxy. In cold molecular clouds, layers of ice form on the surface of dust grains. The main constituent of ice in envelopes of YSOs is H₂O, mixed primarily with CO and CO₂.⁶³ Since the H₂O ice abundances ($\sim 10^{-4}$; e.g., refs 64 and 65) exceed by a few orders of magnitude the gas-phase abundances, understanding gas–grain processes is crucial to fully understand the chemistry in the YSO envelopes.

In the LMC and by comparison to Galactic samples, CO₂ ice column densities are enhanced with respect to H₂O ice,^{58,60,62} while relative CO-to-CO₂ abundances are unchanged.¹¹ The authors of ref 11 proposed the scenario where the high CO₂/H₂O ratio is due to the low abundance of H₂O in the LMC. If there is a difference in the optical extinction A_V threshold for H₂O and CO₂ ices (as the observations suggest), there could be an envelope of less shielded material that shows H₂O ice but no CO₂ ice. The strong interstellar radiation in the LMC penetrates deeper into the YSO envelopes as compared with Galactic YSOs, possibly destroying H₂O ice in less-shielded outer layers without affecting CO₂ and H₂O ice mixtures that exist deeper in the envelope.

In their Very Large Telescope (VLT)'s "Infrared Spectrometer And Array Camera" (ISAAC) near-infrared spectroscopic observations, the authors of ref 66 marginally detected CH₃OH ice absorption band toward two embedded massive YSOs in the LMC with the abundances suggesting that solid CH₃OH is less abundant for high-mass YSOs in the LMC than those in the Galaxy. They proposed a model which explains both the low abundance of CH₃OH and the higher abundance of solid CO₂ found in previous studies. In this "warm ice chemistry" model, the grain surface reactions at a relatively high temperature ($T \gtrsim 20$ K) are responsible for the observed characteristics of ice chemical composition in the LMC. The high dust temperature in the low-metallicity environment caused by the strong interstellar radiation field leads to inefficient H atom sticking and CO hydrogenation to CH₃OH on grain surfaces. At the same time, the production of CO₂ is enhanced as a result of the increased mobility of parent species (CO and OH; see section 5.2.1 for a discussion on theoretical models).

The *Spitzer*/IRS spectroscopy also revealed several COMs in the *circumstellar* environment of SMP LMC 11 (or LHA 120-N78), an object in the LMC classified as a carbon-rich planetary nebula (PN) in the optical, but with infrared properties consistent with it being in the transition from the post-asymptotic giant branch (AGB) to the PN stage (e.g., ref 67 and references therein). The authors of ref 67 identified the diacetylene (C₄H₂), ethylene (C₂H₄), triacetylene (C₆H₂), benzene (C₆H₆), and possibly methylacetylene (CH₃C₂H; commonly known as propyne which is found also in Titan's atmosphere) absorption bands in the *Spitzer*/IRS spectrum of SMP LMC 11. C₆H₆ is a simplest building block of PAHs, which are abundant and ubiquitous in the interstellar medium (e.g., ref 68). In the subsequent analysis and modeling of the same *Spitzer*/IRS spectrum, the authors of ref 69 questioned the detection of C₆H₂, but confirmed the detection of CH₃C₂H. SMP LMC 11 shows a peculiar chemistry, not typical for PN or post-AGB objects in general; e.g., it is one of only two evolved stars in which hydrocarbons up to benzene in absorption are detected (e.g., refs 69–71).

4. THE QUEST FOR DETECTING COMs IN THE MAGELLANIC CLOUDS WITH ALMA

The detection of CH₃OH and more complex molecules in the Magellanic Clouds has been accelerated by the advent of ALMA.

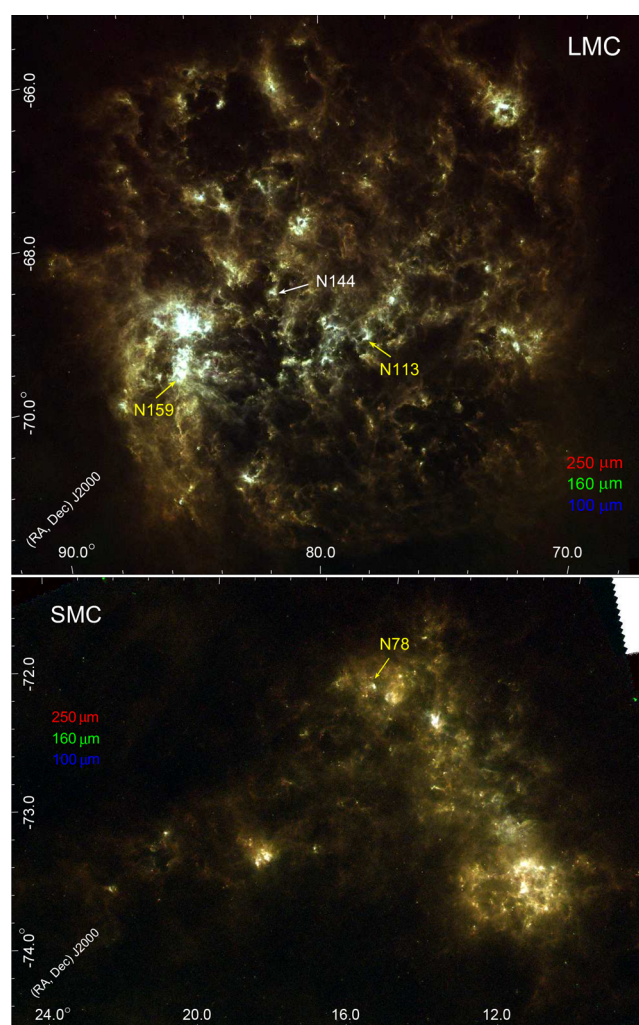


Figure 1. Three-color composite mosaics of the LMC (top) and SMC (bottom), combining the *Herschel*/HERITAGE 250 μm (red), 160 μm (green), and 100 μm (blue) images.²¹ Star-forming regions harboring sources with the detection of COMs (N113 and N159 in the LMC and N78 in the SMC; see Table 2) are indicated with yellow arrows and labeled. The location of the star-forming region N144 hosting ST11, a hot core without COMs, is indicated in white. North is up and east to the left.

ALMA provides high spatial resolution and sensitivity, which enabled studies in the LMC/SMC that in the pre-ALMA era were only possible in our Galaxy. The wide frequency coverage of ALMA observations (up to four ~ 2 GHz spectral windows in the sub-mm/mm wavelength range) allows for simultaneous observations of multiple molecular species and enables serendipitous discoveries.

4.1. Hot Core without COMs: LMC ST11. ST11 is a high-mass YSO ($\sim 5 \times 10^5 L_\odot$, *Spitzer* YSO 052646.61-684847.2,^{47,48,54,62,72} or IRAS 05270-6851) located in the N144 star-forming region in the LMC (Figures 1 and 2). In the pre-ALMA era, the spectral properties of the source were well studied with mid-infrared and near-infrared spectroscopy, which have detected absorption bands due to H₂O ice, CO₂ ice, and silicate dust, as well as emission due to PAHs and hydrogen recombination lines.^{62,72}

The high-resolution (~ 0.5 or ~ 0.12 pc) sub-millimeter (~ 0.86 mm) observations toward ST11 with ALMA revealed the presence of a hot molecular core associated with the

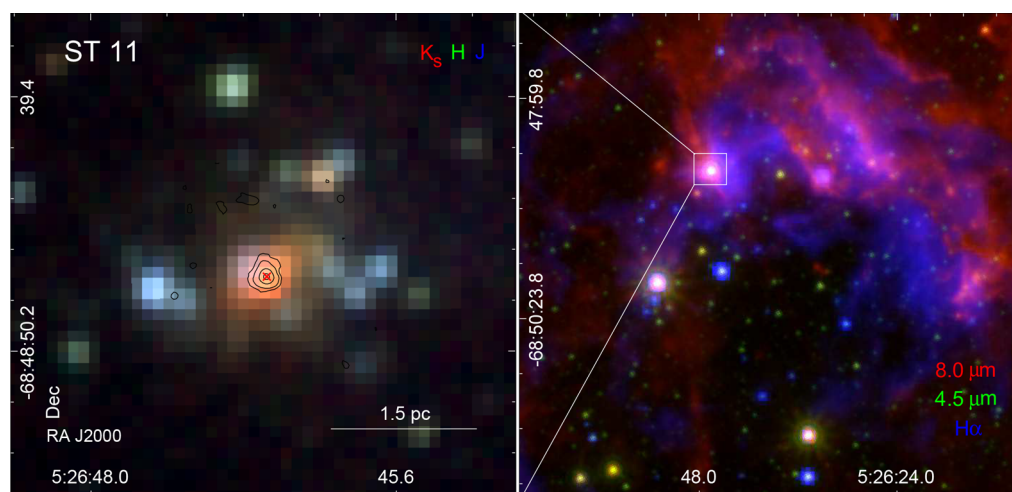


Figure 2. *Left:* Three-color mosaic combining the InfraRed Survey Facility (IRSF) K_s (red), H (green), and J (blue)⁷⁴ images for the LMC source ST11: the source with a hot-core chemistry, but no COMs detection.⁷³ *Right:* A three-color mosaic combining the Spitzer/SAGE 8.0 μm (red) and 4.5 μm (green) images⁴⁵ and the MCELS $H\alpha$ (blue) image.⁷⁵ The ALMA 840 μm continuum contours are overlaid on the image in the left panel; the contour levels are $(3, 6, 20, 40) \times 0.94 \text{ mJy beam}^{-1}$, the 840 μm image rms noise level. The ALMA beam size is $0''.5 \times 0''.5$. The red \times symbol in the left panel indicates the position of the Spitzer YSO: the bright source in the mosaic shown in the right panel.

source.⁷³ According to the rotational diagram analysis of multiple $^{32}\text{SO}_2$ and $^{34}\text{SO}_2$ lines, the gas temperature of the hot-core region is estimated to be $\sim 100\text{--}200 \text{ K}$. The total gas density of the source is estimated to be higher than $2 \times 10^6 \text{ cm}^{-3}$ based on the analysis of the sub-millimeter dust continuum. Emission lines of CO , C^{17}O , HCO^+ , H^{13}CO^+ , H_2CO , NO , H_2CS , ^{33}SO , $^{33}\text{SO}_2$, and SiO are also detected from the compact region associated with the source. High-velocity components are detected in the line profile of CO (3–2), which suggests the presence of molecular outflow in this source.

CH_3OH and larger COMs are not detected toward ST11, despite the high gas temperature that is sufficient for the ice sublimation and despite the detection of H_2CO , a small organic molecule. The estimated upper limit on the CH_3OH gas fractional abundance of 8×10^{-10} is significantly lower than those of Galactic hot cores by a few orders of magnitude⁷³ (see Table 3). The authors of ref 73 hypothesized that the inhibited formation of CH_3OH on the dust surface before the hot-core stage could be responsible for this deficiency. They also estimated upper limits on fractional abundances with respect to H_2 for $(\text{CH}_3\text{OCH}_3)$, (HCOOCH_3) , and $(\text{C}_2\text{H}_5\text{OH})$ of $(<1.5 \times 10^{-8}, <1.8 \times 10^{-8}, \text{ and } <3.7 \times 10^{-9})$. These upper limits indicate that, in ST11, the fractional abundance of CH_3OCH_3 is at least an order of magnitude lower than that in Galactic hot cores, while the HCOOCH_3 and $\text{C}_2\text{H}_5\text{OH}$ fractional abundances are comparable to the average abundances observed in the Galactic counterparts.

4.2. Cold Methanol: LMC N159W-South and SMC IRAS 01042-7215. **4.2.1. N159W-South.** The N159 star-forming region located south from 30 Doradus is one of the best studied areas in the LMC, hosting H II regions, young stellar clusters, Spitzer and Herschel massive YSOs, and a water maser (e.g., ref 49 and references therein; see also ref 42). As described in section 2, N159 was the target of detailed spectral line observations with single-dish telescopes. It is the brightest region in the LMC in ^{12}CO at SEST/Mopra resolution. One of the three giant molecular clouds in N159, N159W, is one of only two regions with a CH_3OH detection in the pre-ALMA era.

The first high-resolution ($\sim 1''$ or $\sim 0.25 \text{ pc}$) ^{13}CO and ^{12}CO (2–1) ALMA observations of N159W resolved the molecular

gas emission into filaments and detected two sources with outflows.⁷⁷ It was the first detection of both filamentary structure and outflows outside the Galaxy. These observations identified two main regions of high-mass star formation, which were dubbed N159W-North and N159W-South (or N159W-N and N159W-S, respectively). Both N159W-N and N159W-S are associated with Spitzer/Herschel YSOs.^{47–49,51,54} Two Stage 0/I YSOs with outflows have masses $>30 M_\odot$ and are associated with 1.3 mm continuum peaks, one in each N159W-N (YSO-N or Spitzer 053937.56-694525.4) and N159W-S (YSO-S or Spitzer 053941.89-694612.0; e.g., ref 49). Based on the kinematics of the molecular gas and the location of YSO-S at the intersection of two ^{13}CO filaments, it was proposed that star formation in N159W-S was triggered by the collision of two filaments $\sim 10^5$ years ago.⁷⁷

This model was revised in ref 76, based on the 4 times higher resolution observations of CO isotopes ($\sim 0''.25$ or 0.06 pc), which resolved the filaments in N159W-S into a complex, hub-filament structure. Multiple protostellar sources with outflows separated by $0.2\text{--}2 \text{ pc}$ were detected along the main massive filament. They correspond to the three major 1.3 mm continuum peaks dubbed MMS-1, MMS-2, and MMS-3 (see Figure 5). The observations in ref 76 are consistent with a scenario in which a large-scale ($>100 \text{ pc}$), rather than local ($\sim 10 \text{ pc}$; see ref 77), collision triggered the formation of both filaments and massive protostars in N159W-S.

MMS-1 and MMS-2 continuum sources are associated with two near-infrared sources, N159 A7 “121” and “123”, respectively, detected as reported in ref 78 using high-resolution ($\sim 0''.2$) VLT/NACO observations. The position of the Spitzer YSO (YSO-S in ref 77; see Figure 3) is offset to the west, hinting at the possibility that a cluster is being formed. No infrared source is detected toward MMS-3, indicating that it is the youngest of the three protostars. Recent VLT/KMOS observations (a pixel scale $0''.2$, a full width at half-maximum seeing $\sim 0''.4$; PI Jacob Ward, see section A.2 for technical details) targeting YSO-S (see Figure 3) detected the K -band continuum, the Brackett- γ emission line of hydrogen ($\text{Br}\gamma$), and the H_2 emission line toward N159 A7 121 (MMS-1) and 123 (MMS-2). As the H_2 and $\text{Br}\gamma$ lines trace shocks and

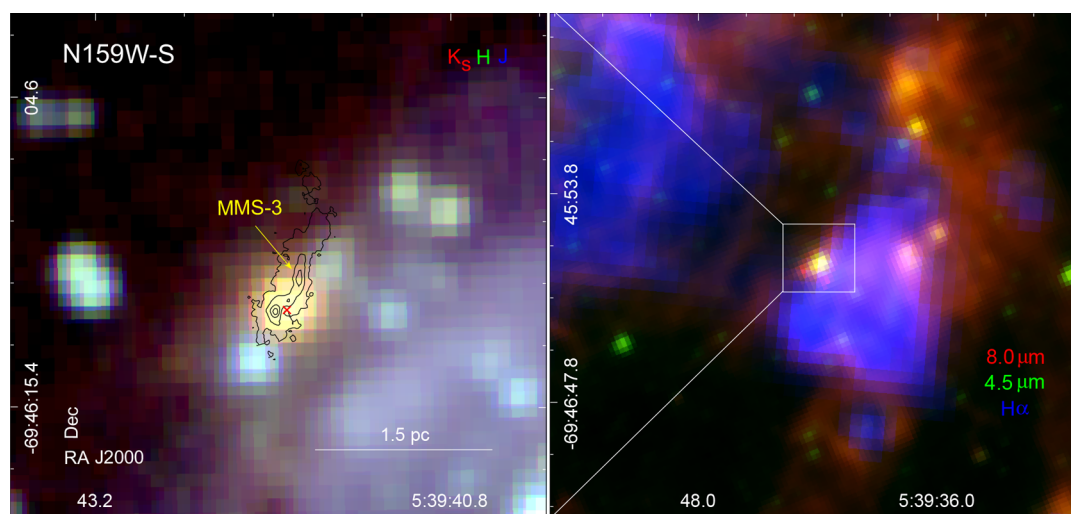


Figure 3. Same as Figure 2, but for N159W-S: the source with a cold methanol detection (PI Peter Schilke, see sections 4.2.1 and A.1). The ALMA 1.3 mm continuum contours are overlaid on the image in the left panel; the contour levels are (0.1, 0.3, 0.5, 0.7) mJy beam⁻¹, the image rms noise level is 0.027 mJy beam⁻¹.⁷⁶ The ALMA beam size is 0".26 × 0".23.

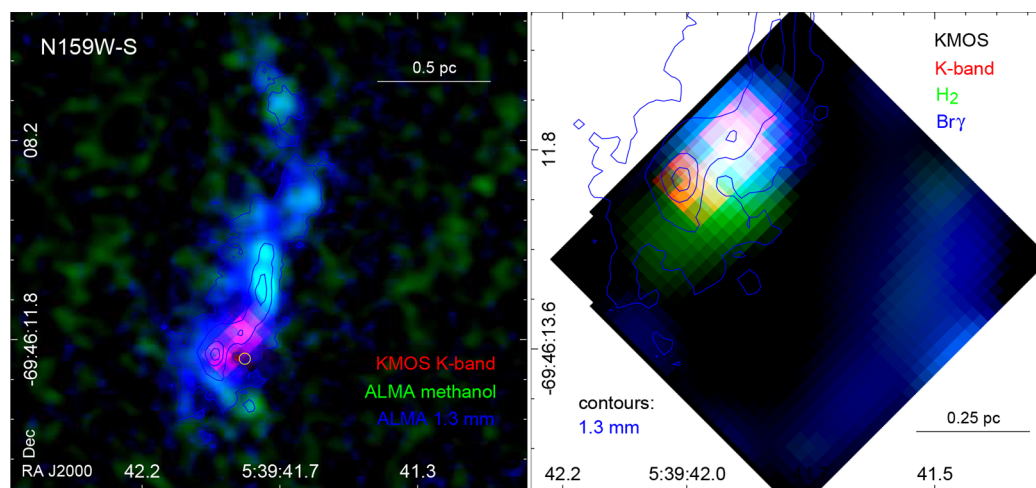


Figure 4. Left: Three-color mosaic combining the VLT/KMOS K-band (red), ALMA CH₃OH (green), and ALMA 1.3 mm (blue) images of N159W-S. The contours correspond to the 1.3 mm continuum emission with contour levels the same as in Figure 3. The yellow circle shows the catalog position of the Spitzer YSO.⁴⁸ Right: Three-color mosaic combining KMOS images: K-band (red), H₂ (green), and Brγ (blue). The 1.3 mm continuum contours (the same as in the left panel) are overlaid for reference.

accretion, respectively, they can shed light on the nature of the sources and thus possible formation scenarios of COMs (e.g., non-thermal origin in shocks traced by H₂). The right panel in Figure 4 shows a combination of the three KMOS images with the ALMA continuum contours overlaid for reference. The extended H₂ emission is associated with outflows from N159 A7 121 (MMS-1) and 123 (MMS-2) detected with ALMA.⁷⁶ The Brγ emission is only detected toward N159 A7 123 (MMS-2).

The most recent ALMA observations of N159W-S detected multiple CH₃OH peaks throughout the region (see Figure 5; PI Peter Schilke), with the brightest emission associated with the continuum source MMS-3. The left panel in Figure 4 shows a three-color mosaic combining the KMOS K-band, ALMA CH₃OH, and 1.3 mm continuum emission. No CH₃OH emission is detected toward MMS-1 and MMS-2 that have infrared counterparts. Although these observations were designed to detect multiple COMs (e.g., CH₃OH, CH₃CN (methyl cyanide), HCOOCH₃, CH₃OCH₃), only CH₃OH was found. The detection of multiple peaks hints at the possibility

that there is an underlying, more extended distribution of CH₃OH that is resolved out.

Preliminary local thermodynamic equilibrium (LTE) fitting using multiple CH₃OH lines (~241.7–241.9 GHz; see Table 5 below) detected toward the two brightest peaks indicate that the gas is cold (~14 K). Methanol forms on grain surfaces and has to be released to the gas phase by energetic events to be detectable. The desorption mechanisms include sublimation by infrared heating by a forming star, photodesorption by UV photons, sputtering by shocks, and chemical desorption (see a discussion in section 5). None of these mechanisms is directly supported by the observations of N159W-S: the gas is cold (desorption by the infrared and UV heating is less likely) and the line widths are narrow (broad lines are expected in the shock sputtering scenario). Moreover, the average cosmic ray flux in the LMC is low, making the cosmic-ray-induced UV radiation less effective than in the Galaxy. Since the analysis of the ALMA CH₃OH data is preliminary, we do not provide physical parameters for N159W-S in Table 2.

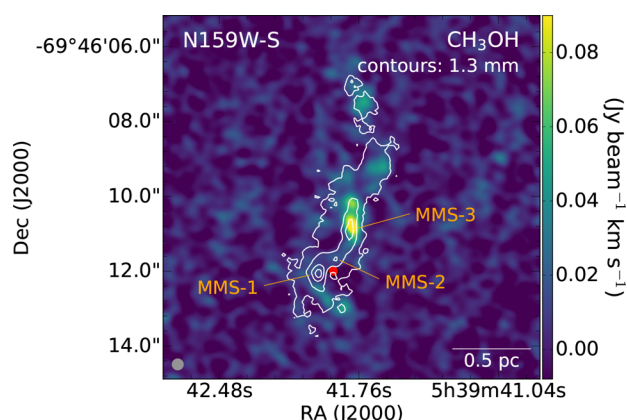


Figure 5. Integrated intensity image of CH₃OH for N159W-S, with the 1.3 mm continuum contours and the positions of the continuum peaks (MMS-1, MMS-2, and MMS-3)⁷⁶ overlaid. The position of the *Spitzer* YSO is indicated with the red filled circle (e.g., ref 49). The 1.3 mm continuum contour levels and the ALMA beam size are the same as in Figure 3. The ALMA synthesized beam size of the CH₃OH observations (shown in the lower left corner) is 0."3 × 0."3.

4.2.2. IRAS 01042-7215. IRAS 01042-7215 is a high-mass YSO ($\sim 2 \times 10^4 L_{\odot}$; e.g., refs 11 and 79; *Spitzer* YSO SSTISAGEMA J010549.30-715948.5, ref 52) located in the northeast region of the SMC bar at the outskirts of the N78 star-forming region (see Figures 1 and 6). The source is well studied through near-infrared and mid-infrared spectroscopy; absorption bands due to H₂O ice, CO₂ ice, and silicate dust are detected, while prominent PAH bands and ionized metal lines are not detected.^{10,11,59,79} No CH₃OH ice has been detected toward IRAS 01042-7215.

Recent VLT/SINFONI K-band observations (a pixel scale of 0."1, a full width at half-maximum seeing $\sim 0."6$)⁸⁰ detected the Br γ and H₂ emission lines toward IRAS 01042-7215.⁸⁰ Figure 7 shows a three-color mosaic combining the SINFONI K-band continuum, H₂, and Br γ images. The SINFONI image reveals a single compact embedded source ($A_v = 16 \pm 8$ mag) with little or no extended line emission. The measured H₂ emission line ratios are consistent with expectations for shocked emission.⁸¹

The high-resolution ($\sim 0."22$ – $0."37$ or ~ 0.07 – 0.11 pc at the distance of the SMC) 1.2 mm ALMA observations detected two continuum peaks, P1 and P2/P3, toward IRAS 01042-7215. P2/P3 is further resolved into two sources (P2 and P3) corresponding to the CH₃OH emission peaks where multiple CH₃OH transitions are detected (Figure 8; see also ref 19).

The 1.2 mm continuum source P1 is associated with the high-mass YSO corresponding to the IRAS source, while no infrared sources are detected at the positions of P2 and P3 (see Figure 7 and ref 19). P2 and P3 correspond to the two CH₃OH emission peaks in the region; no CH₃OH is detected toward P1 (Figure 8 and see also ref 19). Besides CH₃OH, CS, C³³S, SO, SO₂, H¹³CO⁺, H¹³CN, SiO are detected toward P2/P3, but no COMs larger than CH₃OH.

The rotation diagram analysis of the CH₃OH lines for IRAS 01042-7215 P2 and P3 suggests that the temperature of the CH₃OH gas is low (~ 20 K), well below the sublimation temperature of the CH₃OH ice (~ 80 K).⁸² This is another example of a source in the Magellanic Clouds with the detection of "cold methanol". The CH₃OH abundances relative to H₂ for P2 and P3 are an order of magnitude lower than those for hot cores A1 and B3 in N113 (see Table 2 and section 4.3). The origin of CH₃OH gas in P2/P3 is still under debate. The authors of ref 19 suggest that a possible origin could be sputtering of the

Table 2. Positions, Physical Properties, and Fractional Abundances for Sources Described in Section 4 with COMs Detection or Measured Upper Limits with ALMA

source	R.A. (J2000) (h:m:s)	decl (J2000) (°:':")	molecule	T _{rot} (K)	N (cm ⁻²)	N/N(H ₂)	type ^m	ref
LMC								
N113 A1 ^a	05:13:25.17	−69:22:45.5	CH ₃ OH ^g	134 ± 6	(1.6 ± 0.1) × 10 ¹⁶	(2.0 ± 0.3) × 10 ^{−8}	HC	18
			CH ₃ OCH ₃	— ^h	(1.8 ± 0.5) × 10 ¹⁵	(2.2 ± 0.7) × 10 ^{−9}		
			HCOOCH ₃	— ^h	(1.1 ± 0.2) × 10 ¹⁵	(1.4 ± 0.4) × 10 ^{−9}		
N113 B3 ^a	05:13:17.18	−69:22:21.5	CH ₃ OH ^g	131 ± 15	(6.4 ± 0.8) × 10 ¹⁵	(9.1 ± 1.7) × 10 ^{−9}	HC	18
			CH ₃ OCH ₃	— ^h	(1.2 ± 0.4) × 10 ¹⁵	(1.7 ± 0.7) × 10 ^{−9}		
			HCOOCH ₃ ^f	— ^h	<3.4 × 10 ¹⁵	<0.5 × 10 ^{−9}		
N159W-S ^{b,j}	05:39:41	−69:46:06	CH ₃ OH				CM	^k
ST11 ^{c,i}	05:26:46.60	−68:48:47.0	CH ₃ OH	100 ^l	<3.5 × 10 ¹⁴	<8 × 10 ^{−10}	HC*	73
			CH ₃ OCH ₃	100 ^l	<1.3 × 10 ¹⁵	<3 × 10 ^{−9}		
			HCOOCH ₃	100 ^l	<7.1 × 10 ¹⁵	<2 × 10 ^{−8}		
			C ₂ H ₅ OH	100 ^l	<2.2 × 10 ¹⁵	<5 × 10 ^{−9}		
SMC								
IRAS 01042-7215 P2 ^{d,i}	01:05:49.54	−71:59:48.9	CH ₃ OH	18 ± 5	(1.4 ^{+1.1} _{−0.6}) × 10 ¹⁴	(5.0 ^{+4.3} _{−2.3}) × 10 ^{−10}	CM	19
IRAS 01042-7215 P3 ^{e,i}	01:05:49.50	−71:59:49.4	CH ₃ OH	22 ± 6	(1.6 ^{+1.1} _{−0.6}) × 10 ¹⁴	(1.5 ^{+1.0} _{−0.6}) × 10 ^{−9}	CM	19

^aThe positions of N113 A1 and B3 correspond to the ~ 224.3 GHz continuum peaks. ^bMultiple CH₃OH peaks are detected across the N159W-South molecular clump (see section 4.2.1 and Figure 5). ^cThe position of ST11 corresponds to the 359 GHz continuum peak. ^dThe position of IRAS 01042-7215 P2 corresponds to the C³³S, H₂CS, and SiO peaks. ^eThe position of IRAS 01042-7215 P3 corresponds to the CH₃OH peak. ^fA tentative detection. ^g T_{rot} and N were determined using the MADCUBAIJ software with the initial estimates based on the rotational diagram analysis of CH₃OH. ^h T_{rot} for CH₃OCH₃ and HCOOCH₃ was assumed to be equal to T_{rot} determined for CH₃OH. ⁱ T_{rot} and N were determined based on the rotational diagram of CH₃OH; the values presented in the table are the revised values from ref 19, based on new ALMA observations (PI T. Shimonishi). ^jThe analysis of the N159W-South data is preliminary; thus, we do not provide physical parameters for this region. ^kPI P. Schilke. ^lThe average rotation temperature of SO₂, ³⁴SO₂, and ³³SO₂; N and $N/N(\text{H}_2)$ upper limits are at the 2 σ level. ^mType: HC, a hot core; HC*, a hot core with no COMs; CM, a source with cold methanol.

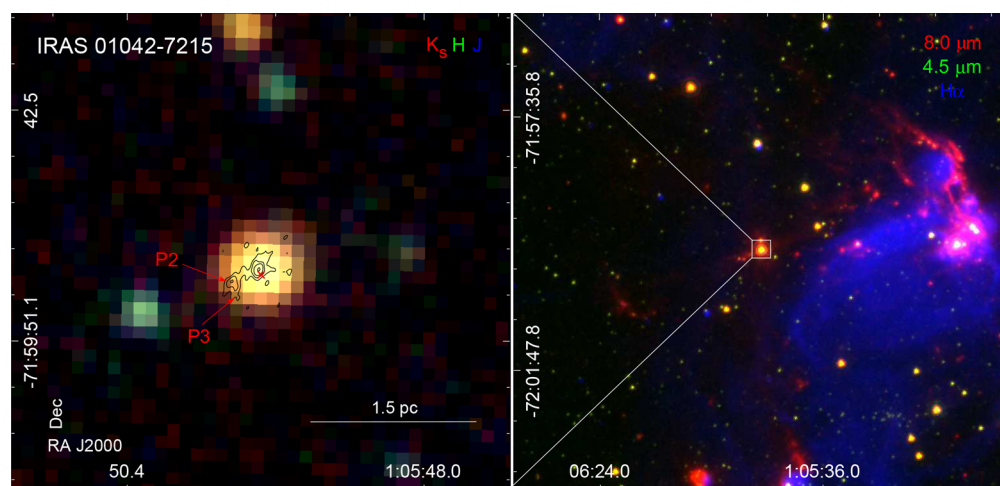


Figure 6. Same as Figure 2, but for the field around the SMC source IRAS 01042-7215, where CH₃OH was detected toward sources P2 and P3 (indicated in the left panel), corresponding to the CH₃OH peaks.¹⁹ The ALMA 1.2 mm continuum contours are overlaid. The continuum contour levels are (3, 6, 10, 20) × 21 mJy beam⁻¹, the 1.2 mm image rms noise level. The ALMA synthesized beam size is 0".35 × 0".22.

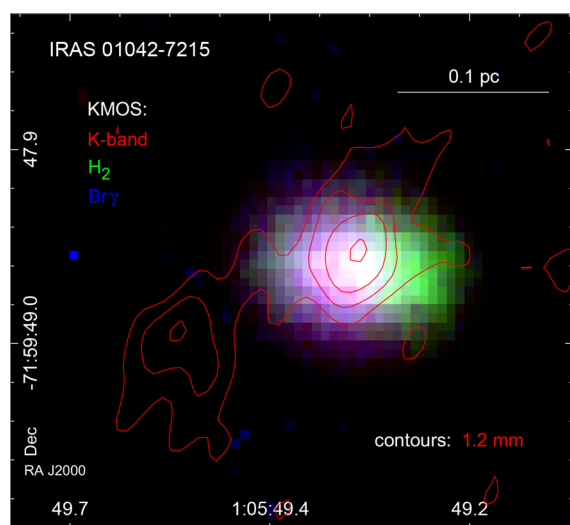


Figure 7. Three-color mosaic of the IRAS 01042-7215 field combining the VLT/SINFONI K-band (red), H₂ (green), and Br γ (blue) images.⁸⁰ Red contours correspond to the ALMA 1.2 mm continuum emission with contour levels the same as in Figure 6.

ice mantles by shocks triggered by the outflow from nearby YSOs, or chemical desorption of CH₃OH from dust surfaces. The presence of shocked but cold CH₃OH gas has been suggested in Galactic infrared dark clouds, indicating that CH₃OH may be tracing relatively old shocks (e.g., ref 83).

4.3. Hot Cores with COMs More Complex than Methanol: LMC N113 A1 and B3. To date, COMs with more than six atoms have only been reliably detected in the Magellanic Clouds toward two sources, both in the LMC N113 star-forming region. The physical and chemical characteristics of N113 make it one of the most interesting star-forming regions in the LMC. Like N159, it was the target of detailed spectral line studies with single-dish telescopes (see section 2) that resulted in the detection of CH₃OH.¹⁷

N113 contains: (1) one of the most massive ($\sim 10^5 M_{\odot}$) and richest GMCs in the LMC;²⁷ (2) signatures of both recent (H α emission) and ongoing (e.g., maser and bright infrared emission) star formation;^{34,84} (3) signatures of star formation triggered by winds from massive stars; (4) the largest number of

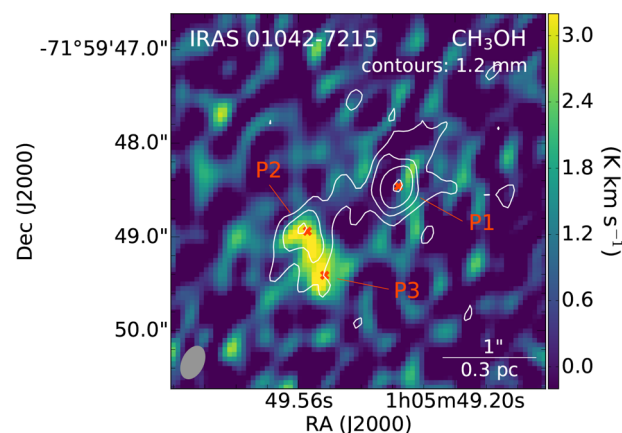


Figure 8. CH₃OH integrated intensity image (the average of the CH₃OH S_{-1,5}–4_{-1,4} E and S_{0,5}–4_{0,4} A⁺ lines) of IRAS 01042-7215 in the SMC. The 1.2 mm continuum contours are overlaid; the contour levels and the size of the ALMA synthesized beam shown in the lower left corner are the same as in Figure 6.

H₂O and OH masers and the brightest H₂O maser in the entire LMC;^{38,42,84–86} and (5) it has among the highest concentrations of *Spitzer*/*Herschel* Stage 0-II YSO candidates in the LMC.^{47,48,51,53,54}

Mid-infrared sources, maser emission, and compact H II regions in the central part of the GMC associated with the extended gas and dust emission, reveal sites of the current star formation in N113 (see Figure 9). The *Spitzer* (3.6–160 μ m) and *Herschel* (160–500 μ m) images with resolutions ranging from $\sim 2''$ to $38''$ show that this region is dominated by three bright sources, which were identified as 30–40 M_{\odot} Stage I YSOs (YSO-1, YSO-3, and YSO-4 in Figure 9: *Spitzer* sources 051317.69-692225.0, 051325.09-692245.1, and 051321.43-692241.5, respectively)⁴⁸ and are characterized by distinct physical conditions (see refs 48 and 87, as well as Oliveira et al., manuscript submitted to Monthly Notices of the Royal Astronomical Society).

Detailed *Spitzer* and *Herschel* studies on the YSO population in N113 were followed by ALMA Band 6 (~ 1.3 mm) observations at 0.18 pc (or $\sim 0''.8$) resolution in the molecular transitions that probe a wide density range (10^2 – 10^7 cm⁻³) to

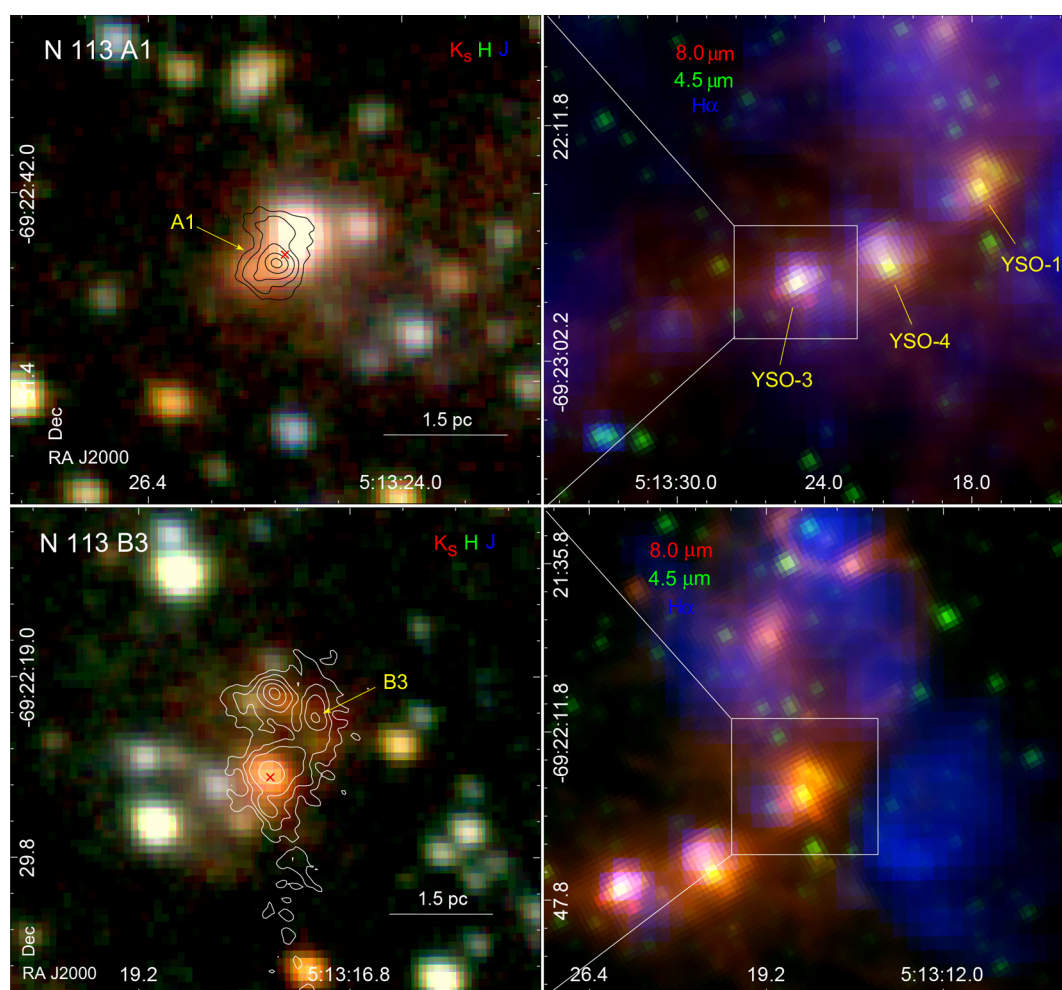


Figure 9. Left: Same as in Figure 2, but for N113 A1 (top) and B3 (bottom) hot cores. The contours in the left panel correspond to the 1.3 mm continuum emission.¹⁸ The contour levels are (5, 10, 20, 50) \times the image rms noise level of 0.1 mJy beam⁻¹.

study both the dense clumps/cores and the lower density gas in the inter-clump regions. The ionized gas and outflow tracers were also included in the program. These observations resulted in a serendipitous discovery of COMs CH₃OH, HCOOCH₃, and CH₃OCH₃ toward two locations in the region¹⁸ (see Figures 9 and 10). The detected transitions are listed in Table 5 below. This was the first conclusive detection of COMs more complex than methanol outside the Galaxy and in a low-metallicity environment. COMs were detected toward two 1.3 mm continuum sources, A1 and B3, in the field around *Spitzer* YSO-3 ("Region A" in ref 18) and YSO-1 ("Region B"). Figure 9 shows three-color mosaics covering A1 and B3 combining near-infrared bands with 1.3 mm contours overlaid, as well as a larger scale environment in N113 traced by the *Spitzer* 4.5 and 8.0 μ m, and H α emission. Figure 10 shows the integrated intensity CH₃OH, CH₃OCH₃, and HCOOCH₃ images of Regions A and B.

A1 and B3 are compact (diameter $D \approx 0.17$ pc) and are associated with H₂O (A1 and B3) and OH (A1) masers. H₂ column densities of $(8.0 \pm 1.2) \times 10^{23}$ and $(7.0 \pm 0.9) \times 10^{23}$ cm⁻² and number densities of $\sim 1.6 \times 10^6$ and $\sim 1.4 \times 10^6$ cm⁻³ for A1 and B3, respectively, were estimated using the 1.3 mm continuum data. The LTE analysis of six CH₃OH transitions resulted in rotational temperatures and total column densities ($T_{\text{rot}} N_{\text{tot}}$) of $(134 \pm 6$ K, $1.6 \pm 0.1 \times 10^{16}$ cm⁻²) and $(131 \pm 15$ K, $6.4 \pm 0.8 \times 10^{15}$ cm⁻²) for A1 and B3, respectively.¹⁸ These

sizes, number and column densities, and temperatures of A1 and B3 are consistent with classic hot cores observed in the Galaxy. COMs emission and association with masers are also among the main characteristics of hot cores. These are the first bona fide detections of complex hot-core chemistry outside the Galaxy.

The (CH₃OH, CH₃OCH₃, HCOOCH₃) column densities are $(16 \pm 1, 1.8 \pm 0.5, 1.1 \pm 0.2) \times 10^{15}$ cm⁻² for A1 and $(6.4 \pm 0.8, 1.2 \pm 0.4, <0.34) \times 10^{15}$ cm⁻² for B3. Column densities for HCOOCH₃ and CH₃OCH₃ were estimated using the same T_{rot} as for CH₃OH, assuming that these molecular species are located in the same region as CH₃OH in A1 and B3.

The (CH₃OH, CH₃OCH₃, HCOOCH₃) fractional abundances with respect to H₂ are $(20 \pm 3, 2.2 \pm 0.7, 1.4 \pm 0.4) \times 10^{-9}$ for A1 and $(9.1 \pm 1.7, 1.7 \pm 0.7, <0.5) \times 10^{-9}$ for B3 (see Table 2). The CH₃OH fractional abundances in A1 and B3 are over an order of magnitude larger than an upper limit estimated for ST11 in ref 73 (see section 4.1). Table 3 lists CH₃OH, CH₃OCH₃, and HCOOCH₃ fractional abundances for a set of Galactic hot cores. When scaled by a factor of 2.5 to account for the lower metallicity in the LMC (the ratio between the solar metallicity and the metallicity of the LMC, assuming $Z_{\text{LMC}} = 0.4 Z_{\odot}$), the abundances of COMs detected in N113 are comparable to those found at the lower end of the range in Galactic hot cores. This was a surprising result because previous observational and theoretical studies indicated that the abundance of CH₃OH in the LMC is very low. The authors of ref 18

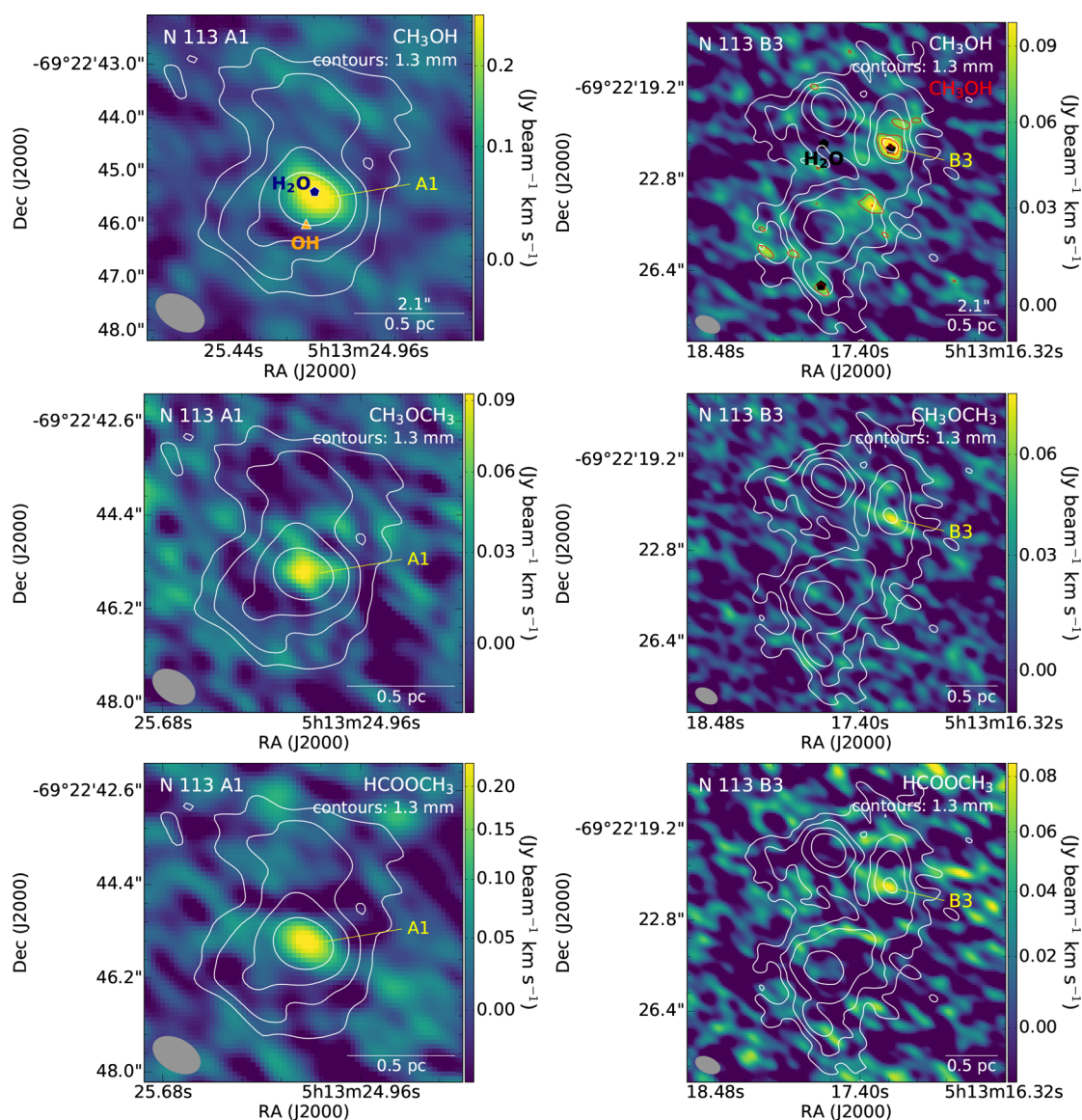


Figure 10. Integrated intensity images for CH_3OH (top panel; made using the channels corresponding to all CH_3OH transitions in the 216.9 GHz spectral window; see Table 5), CH_3OCH_3 (middle panel; the $13_{0,13}-12_{1,12}$ transition); and HCOOCH_3 (bottom panel; integrated over all detected transitions) for the A1 (left column) and B3 (right column) hot cores in the N113 star-forming region. The H_2O and OH masers are indicated. The white contours correspond to the 1.3 mm continuum emission; the contour levels are the same as in Figure 9. The red contours in the top right panel correspond to the CH_3OH emission with contour levels of (3, 5, 7) $\times 21$ mJy beam $^{-1}$, the rms noise level of the CH_3OH integrated intensity image. The image shows the CH_3OH detection in other spots in the region ("Region B" in ref 18) where no other COMs are detected. The results presented in this figure were reported in ref 18. The ALMA beam size is shown in the lower left corner in each image.

concluded that COMs observed in the N113 hot cores could originate either from grain surface chemistry or in post-desorption gas chemistry.

The quartet $J = 2_K-1_K$ of CH_3OH at ~ 96.7 GHz was later detected serendipitously toward N113 with ALMA in the project targeting two transitions ($1-0$ and $2-1$) of three CO isotopes (^{12}CO , ^{13}CO , and C^{18}O) toward three LMC and three SMC star-forming regions with a resolution of $\sim 2''$ (or ~ 0.48 pc). N113 is the only region in this sample with CH_3OH detection. The spectral window with the CH_3OH line was dedicated to the continuum observations and has a spectral resolution of ~ 50 km s $^{-1}$. Such low spectral resolution does not allow for any quantitative analysis, but surprisingly the data revealed several additional well-defined CH_3OH peaks and extended emission in Region B (see Figure 11). The CH_3OH

emission reported in ref 18 was limited to two compact sources (hot cores A1 and B3), with some fainter emission detected in other locations in Region B (see Figure 10); however, it was unclear whether the latter traces physically distinct sources or shocked lobes of the outflows.

In addition to hot cores, the ~ 96.7 GHz CH_3OH emission is detected toward continuum sources B4, B7, and B6 in Region B and D1–D4 located toward the south (Figure 11; Sewilo et al., manuscript in preparation). In Region A, the ~ 96.7 GHz CH_3OH emission peak coincides with hot core A1; however, the emission extends toward the south.

The ~ 96.7 GHz CH_3OH emission peaks in Regions A and B overlap with the SiO ($5-4$) peaks (with some faint extended emission visible throughout Region B, see Figure 12; ref 18 and Sewilo et al., manuscript in preparation), tracing shocks. The

Table 3. Chemical Abundances Relative to H₂ for COMs Detected in the LMC/SMC for Selected Galactic Hot Cores

source	N(X)/N(H ₂)			ref ^a
	CH ₃ OH	HCOOCH ₃	CH ₃ OCH ₃	
Orion Mol. Cloud:				
hot core	1.4×10^{-7}	1.4×10^{-8}	8.0×10^{-9}	92
compact ridge	4.0×10^{-7}	3.0×10^{-8}	1.9×10^{-8}	92
G34.26-0.15:				
NE	8.5×10^{-7}	7.3×10^{-8}	1.4×10^{-7}	92
SE	6.4×10^{-7}	6.8×10^{-8}	8.5×10^{-8}	92
Sgr B2N	2.0×10^{-7}	1.0×10^{-9}	3.0×10^{-9}	92
G327.3-0.6	2.0×10^{-5}	2.0×10^{-6}	3.4×10^{-7}	92
AFGL 2591	7.0×10^{-7}	$<3.2 \times 10^{-7}$	$<1.0 \times 10^{-7}$	93
G24.78 + 0.08	6.5×10^{-7}	7.3×10^{-8}	3.0×10^{-7}	93
G75.78 + 0.34	9.2×10^{-7}	5.9×10^{-8}	1.9×10^{-7}	93
NGC 6334 IRS 1	4.0×10^{-6}	4.6×10^{-7}	2.4×10^{-6}	93
NGC 7538 IRS 1	5.7×10^{-7}	6.7×10^{-8}	$<7.6 \times 10^{-8}$	93
W3 (H ₂ O)	5.4×10^{-6}	2.9×10^{-7}	8.3×10^{-7}	93
W33A	7.3×10^{-7}	9.6×10^{-8}	1.0×10^{-7}	93

^aAnd references therein. For more information on Galactic hot cores, see also, e.g., refs 94–97 and references therein.

same regions are associated with the DCN (3–2) emission, indicating their youth, and are distributed along the dense gas filament. The observational and theoretical studies indicate that the abundance of all deuterated species strongly depends on temperature: it drops rapidly with increasing gas temperature as an object evolves (see, e.g., refs 88–91).

5. THEORY

We can gain some insight as to the origin of the COMs detected in the Magellanic Clouds by comparing observations with current astrochemical theories of Galactic COM production in star-forming regions. Here we briefly review COM formation mechanisms and how they have been applied to low-metallicity environments.

5.1. Complex Molecule Formation in Star-forming Regions of the Milky Way. In the Galaxy, the largest COMs have until now been found primarily in the hot molecular cores associated with massive protostars, as well as with the so-called hot corinos found in regions of low-mass star formation (e.g., ref 95). In cold, dense molecular clouds, some of these organics have been known to be present for quite some time: HNCO, HCOOH, CH₂CO, CH₃CHO, CH₃OH.⁹⁶ More recently, the larger “hot-core” COMs, including CH₃OCH₃ and HCOOCH₃, have also been detected in several cold clouds.^{98–102} These detections have raised several challenges for existing theories of COM formation. These include the long-standing problem of identifying the mechanism responsible for returning ice-mantle molecules to the gas in cold clouds, and the fact that radical reactions on 10 K grains will not occur. In the case of the cold methanol detected in the LMC, it would appear that reactive desorption (i.e., using part of the energy released upon formation) is a plausible explanation.^{103,104}

Hot cores are regions of high gas density and extinction where elevated dust temperatures have led to the sublimation of molecular ice mantles that have previously grown on cold dust grains. The first model of hot-core chemical evolution was

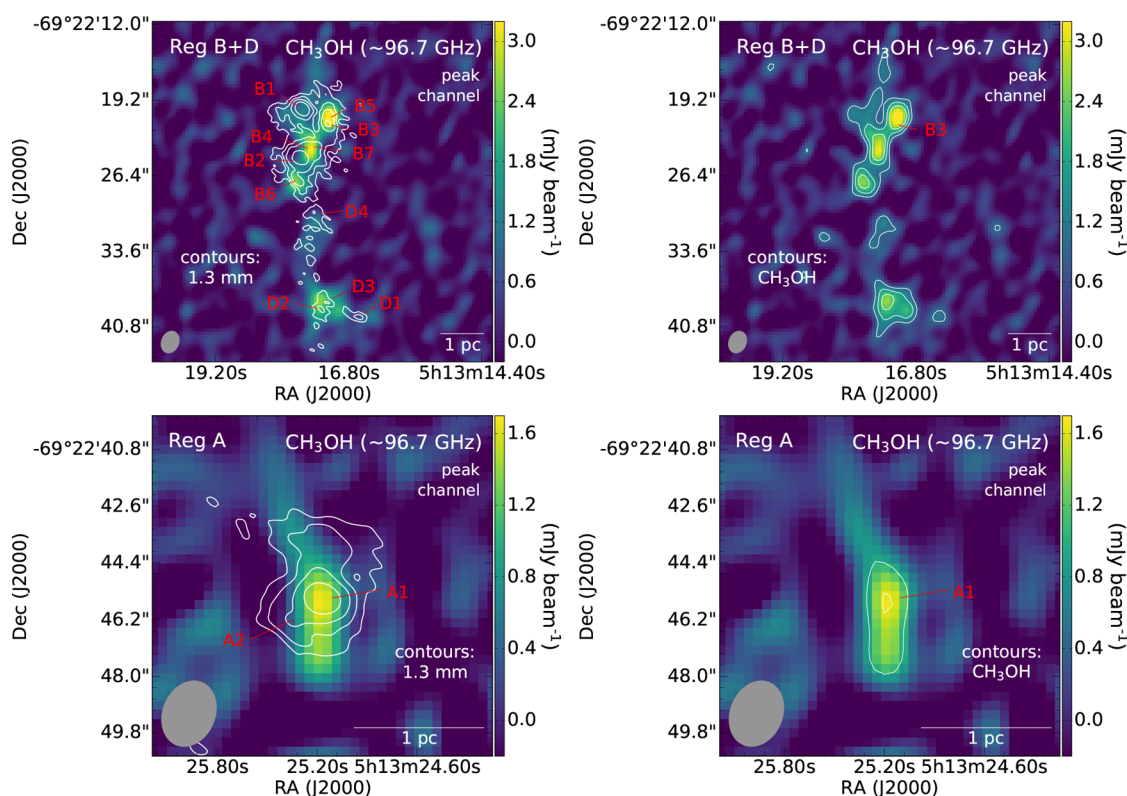


Figure 11. Single-channel maps corresponding to the peak of the unresolved rotational transition quartet $J = 2_K - 1_K$ of CH₃OH at 96.7 GHz for regions in N113 around and south of B3 (top) and toward A1 (bottom) hot cores (Sewilo et al., manuscript in preparation; ALMA 12-m Array data). The white 1.3 mm continuum contours in the left panel are the same as in Figure 9. The white CH₃OH contours in the right panel correspond to $(3, 5, 7) \times$ rms noise level of the CH₃OH single-channel map of $0.32 \text{ mJy beam}^{-1}$. The ALMA beam size ($2''.15 \times 1''.66$) for the CH₃OH observations is shown in the lower left corner in all images.

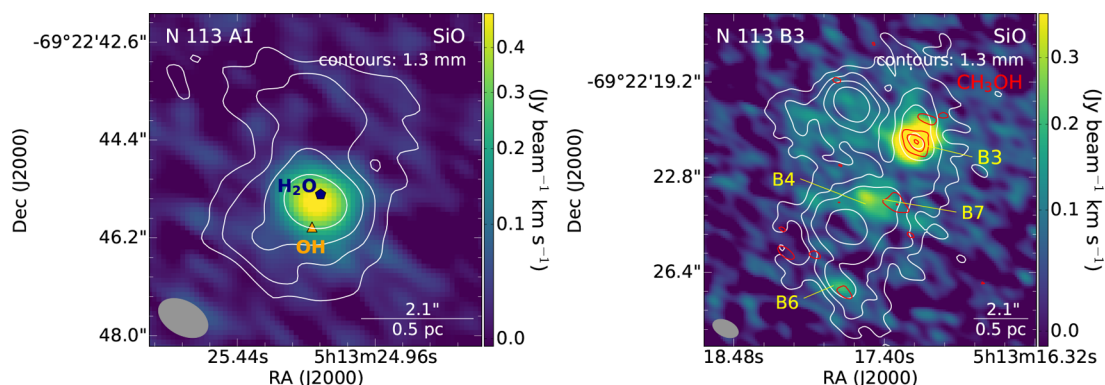


Figure 12. SiO (5–4) integrated intensity images of N113 A1 (left) and B3 (right) hot cores (Sewilo et al., manuscript in preparation). The contours are the same as in Figure 9 (1.3 mm; white) and Figure 10 (CH₃OH; red). The positions of H₂O and OH masers, and 1.3 mm continuum sources associated with the CH₃OH emission are indicated. The ALMA beam size (0.''98 × 0.''61) is shown in the lower left corner in both images.

presented in ref 105. This involves a long period of cold (~10 K) chemistry during which molecules form by gas-phase reactions and on dust grains, as the gas freezes out; this chemistry is similar to that found in cold dark clouds (e.g., ref 106). At some point gravitational collapse ensues, a protostar is formed, and the resulting large increase in luminosity heats the surrounding envelope of gas and dust to temperatures above about 100 K, leading to the sublimation of ice mantles and the formation of the hot core/corino. Further refinements to this picture have been (a) the addition of a slow “warm-up” phase that can allow UV photolysis and radical–radical reactions to occur in the ice mantles, prior to formation of the hot core proper,¹⁰⁷ and (b) gas-phase synthesis in the hot core, driven by the sublimated molecules.¹⁰⁸ Further refinements have included the spatio-temporal evolution of the gas–grain chemistry.^{109,110}

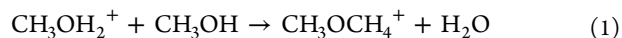
Thus, within this simple picture, the complex molecules observed in hot cores can have four chemical origins: (1) formation in cold gas followed by freeze-out on dust; (2) formation on the surfaces of cold (10 K) dust grains; (3) formation in UV-photolyzed ice mantles at ~30 K; or (4) *in situ* formation in hot-core gas following ice sublimation.

5.1.1. Cold Gas-Phase Reactions in Dark Clouds. Cosmic-ray ionization of molecular hydrogen drives dense cloud chemistry by initiating sequences of ion–neutral and neutral–neutral reactions. This chemistry leads to the production of CO and many of the simple molecules detected in dark interstellar clouds. The complex molecules produced tend to be long hydrocarbon chains and associated radicals, such as the cyanopolyynes and various carbenes. The dark cloud TMC-1 in Taurus is recognized as the best example of this chemistry (e.g., ref 111), and chemical modeling demonstrates that gas-phase chemistry can account quite well for its composition (e.g., ref 112). It is now appreciated that methanol is formed entirely on dust grains (see section 5.1.2), and so some (non-thermal) desorption mechanism is required to explain its presence in dark clouds like TMC-1, since dust temperatures are never sufficiently high for methanol and water to desorb. However, in dense cores where low-mass protostars are forming, it appears that some dust heating (to ~30–35 K) has occurred, and this can lead to the sublimation of more-volatile molecules. In this Warm Carbon Chain Chemistry (WCCC), sublimation of large abundances of methane from the ice mantles greatly increases the efficiency of carbon-chain growth.¹¹³ Although we do not discuss CH₄ injection further, the similarly warm dust

temperatures found in the Magellanic Clouds may make this a viable route to widespread carbon chain formation there.

5.1.2. Cold Grain–Surface Reactions. Ice mantles grow on cold dust grains through the sticking of atoms of O, C, and N followed by reactions with H atoms to form H₂O, CH₄, and NH₃. Molecules formed in the gas, such as CO and N₂, can also accrete and become incorporated in the mantle. Unsaturated molecules can undergo (tunneling) addition reactions with hydrogen atoms to produce molecular radicals that can further react and form new molecules (e.g., ref 114). Figure 13 shows that, in the case of CO, these processes can lead to a rich organic chemistry (e.g., ref 115) through the growth of linear chains by single atom additions and their subsequent saturation. This surface scheme can explain the presence of CH₃OH and many of the COMs known in hot cores and originally made predictions¹¹⁶ for new surface molecules (not shown) that were subsequently detected: glycolaldehyde,^{117,118} ethylene glycol,¹¹⁹ acrolein, and propionaldehyde.¹²⁰ Numerous surface chemistry experiments have validated many of these addition processes.^{121–123}

5.1.3. COM Chemistry Driven by Sublimated Ice Mantles. The authors of ref 108 demonstrated that differences in mantle composition could, following sublimation, account for the chemical differentiation seen in the Orion-KL star-forming region. Rather than calculate the mantle composition *ab initio*, they assumed a composition based on observations and showed that the relative presence, or not, of methanol and ammonia could drive different chemistries in the hot gas (see also refs 124 and 125). In ref 126, it was first suggested that self-methylation of methanol could be the source of dimethyl ether in hot cores, although the authors attributed its origin to be protostellar outflows rather than grain–surface chemistry. The self-methylation reaction is



where the neutral CH₃OCH₃ molecule is produced in reactions with either an electron or a base, such as ammonia. The authors of ref 127 showed, based on laboratory experiments, that apart from CH₃OCH₃, many more large ethers and esters could be formed in this manner, in reactions involving ethanol, propanol, and butanol.¹²⁸ Figure 13 includes alkylation reactions between protonated methanol and ethanol, the neutral alcohols, and formic acid. Methyl formate formation by methylation of HCOOH has also been studied in the laboratory¹²⁹ and shown to be a viable mechanism. In these experiments, the *trans*-

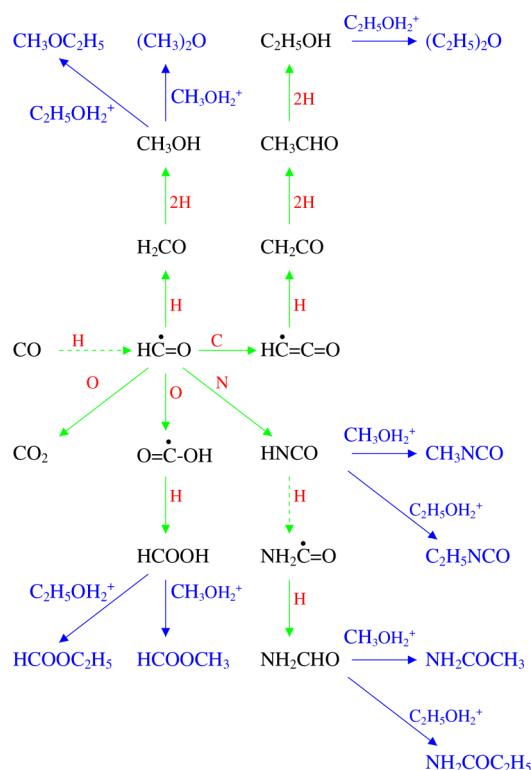


Figure 13. Interstellar gas–grain surface chemistry. Molecules involved in surface reactions are in black. Hydrogen atom addition to unsaturated molecules creates reactive radicals and additions of C, O and N atoms, allows a rich organic chemistry seeded by carbon monoxide to develop. Broken arrows indicate reactions with activation energy barriers; where 2H is shown, a barrier penetration reaction followed by an exothermic addition is implicitly indicated. Once these ice mantles have been sublimated into the hot-core gas, methanol and ethanol can become protonated and take part in ion–molecule alkyl cation transfer reactions with themselves and with other molecules that were formed in the ices. These processes are denoted in blue, and each arrow indicates the initial ion–molecule reaction and the production of the neutral COM, through either electron dissociative recombination or proton transfer to ammonia (adapted from ref 115 and references therein).

HCOOH conformer of formic acid produced the protonated form of *trans*-HCOOCH₃; electron dissociative recombination, or proton transfer (see below), would then lead to the neutral ester. However, apart from one detection of *trans*-HCOOCH₃,¹³⁰ it is the more stable *cis*-HCOOCH₃ conformer that is found in hot cores. It has therefore been suggested that interconversion between *trans*-HCOOCH₃ and *cis*-HCOOCH₃ structures could occur in the proton loss process.¹³¹ Chemical models have demonstrated that this is a very competitive pathway to HCOOCH₃ around protostars,¹³² assuming that interconversion proceeds with high efficiency.¹³³ Of the COM products shown in Figure 13, apart from dimethyl ether and methyl formate, both ethyl formate and ethyl methyl ether have now been detected.^{134,135}

A problem with this scenario has been that experiments on electron dissociative recombination of protonated COMs show that recovery of the neutral molecule occurs with a probability much lower than previously assumed, typically <5% as compared to 100% (e.g., ref 136), and subsequently to COM abundances much lower than observed. However, if NH₃ is injected from grain mantles at moderate abundances, com-

parable with those measured in Galactic ices,¹³⁷ then proton transfer, e.g.,



can dominate COM formation and mitigate against the destructive effects of electron recombinations.^{132,138}

As also shown in Figure 13, gas phase COM formation driven by alkyl cation transfer reactions involving surface-formed HNCO and NH₂CHO could plausibly be a source of new molecules, perhaps explaining the hot-core detections of methyl isocyanide (CH₃NCO) and acetamide (NH₂COCH₃).^{139,140} However, the associated gas phase reactions have not yet been studied experimentally or theoretically and so should be regarded as speculative.

5.1.4. Radical Reactions in Icy Grain Mantles. As well as chemical reactions on grain surfaces driven by accretion of reactive species, it is also known that the ices can undergo bulk processing due to radiation damage caused by photons and energetic particles. Cosmic rays interact directly with icy mantles and recently chemical models have been developed to explore their effects on COM formation (see ref 141 and references therein). The environment of young protostars receives large doses of UV and EUV radiation.¹⁴² Even in dark clouds, a weak ambient flux of internal UV photons will exist¹⁴³ as energetic electrons produced by cosmic-ray ionization of molecular hydrogen can subsequently collide with, and excite, other H₂ molecules which undergo de-excitation by emission of Lyman and Werner band photons. The resulting UV flux is $\sim 10^3$ photons s⁻¹ cm⁻², which can be significant for chemistry in dense clouds. Laboratory experiments on UV photolysis of interstellar ice analogs show that an extensive organic chemistry can occur, primarily through reactions involving various radicals produced from the major (parent) ice species (e.g., ref 144). Cold H additions to CO (see section 5.1.2) have also to be considered since interstellar organic synthesis by photolysis requires that the methanol be present *ab initio*.^{144,145}

Early theoretical models for organic synthesis from the recombination of radicals on cold grains appealed to physically unrealistic processes to attain the high mobilities needed for heavy particle migration and reaction.^{146–150} Detailed modeling has shown that sustained UV photolysis and warming during the early stages of hot-core evolution can produce many new organics.¹⁰⁷ In this picture, the ices are subjected to the Prasad–Tarafdar UV photons during the initial cold phase of core formation, producing a population of radicals. This irradiation can continue as the core is being gradually (as opposed to instantaneously) heated—the so-called “warm-up” phase.^{107,151} When the dust grain temperature reaches, and can be maintained close to, about 30 K, the associated increase in radical mobility allows them to migrate and react. Radical–radical recombinations between HCO, CH₃O, CH₂OH, COOH, and other simple radicals (e.g., CH₃, CH₂, NH₂, CN, OH) then produce many of the COMs observed in hot cores.^{134,152,153}

5.2. Models of COM Formation in the Magellanic Clouds. Here we summarize and discuss theoretical models of COM formation at reduced metallicity in the light of recent observations.

5.2.1. Chemical Models of the LMC and SMC. The authors of ref 154 considered the chemical evolution of putative dark clouds in the LMC and SMC at the appropriate elemental depletions. They considered the purely gas-phase chemistry of fairly simple molecules, with only CH₃OH and CH₂CO being

the only COMs. These models could produce CH_3OH abundances of $\sim 10^{-8}$; however, the main formation mechanism was through a radiative association process that is no longer considered viable.

More recently, gas–grain models of the LMC and SMC were developed.^{155,156} Again, cold dark clouds were modeled for a wider range of physical parameters, including appropriately warmer gas and dust temperatures. In these models CH_3OH was formed by CO hydrogenation on dust grains. For the LMC, they found that molecular abundances similar to Milky Way dark clouds could be obtained, whereas for the SMC the abundances were lower for most molecules. The model predictions were compared to several star-forming regions in the LMC (as no data on Magellanic dark clouds then existed): N159W, N159S, N160, and 30 Dor-10. When compared to the Magellanic source N159W with a thermal methanol detection, the calculated abundances were found to be ~ 10 – 10^3 times lower than determined in ref 16. The reason for this discrepancy was explained as being due to the warm dust temperatures, appropriate for Magellanic dark clouds, that were considered in the models. Dust temperature affects grain-surface chemistry and can inhibit methanol formation since, for temperatures above about 15 K, hydrogen atoms will desorb before they can react with CO. Above about 25 K, CO molecules residing in CO-rich outer layers of the ice mantle will also sublime, whereas those trapped in the H_2O ice matrix require higher dust temperatures.¹⁵⁷ In both the LMC and SMC models, gaseous NH_3 abundances of $\sim 10^{-8}$ were found. For models with dust temperatures more similar to the Milky Way (~ 10 – 15 K), the dust ice mantles are predicted to contain large fractions of CH_3OH (~ 10 – 40%) and NH_3 (~ 1 – 7%). Hence, the presence of CH_3OH in the Magellanic Clouds points to formation in a cold pre-hot-core phase.

The authors of ref 158 studied the formation of ice mantles in the Magellanic Clouds but instead employed a correct stochastic calculation of the grain chemistry. The relative composition of ices comprising of H_2O , CO, CO_2 , CH_3OH , NH_3 and CH_4 were calculated as a function of the interstellar UV radiation field. The CH_3OH and NH_3 ice fractions were found to be lower ($\sim \text{few } \%$) than those reported in refs 155 and 156, and more compatible with those of Galactic ices (ref 137).

The authors of ref 159 reported the first *bona fide* hot-core models of the Magellanic Clouds. Their model was a standard three-phase model (cold quasi-static phase, collapse phase with or without “warm-up”, and hot-core phase; see section 5.1) and included the radical chemistry induced during the “warm-up” phase as well as many of the COMs known in Galactic hot cores (refs 107 and 152; see section 5.1.4). When compared to the N113 observations, only one of the models (a 100 K core in which the initial phase of core formation proceeded at 10 K, Model 1) reproduced the observed CH_3OH abundances in both A1 and B3 at times (post-sublimation) when CH_3OCH_3 and HCOOCH_3 had non-trivial abundances. As CH_3OH is the proposed parent of CH_3OCH_3 and HCOOCH_3 both in grain–surface reactions (see section 5.1.4) and in ion–molecule reactions (see Figure 13), the comparison of predicted $\text{CH}_3\text{OCH}_3/\text{CH}_3\text{OH}$ and $\text{HCOOCH}_3/\text{CH}_3\text{OH}$ ratios with observations provides the most stringent tests of their origin (see section 5.2.2).

Overall, these models indicate that the hot cores in the Magellanic Clouds must have undergone a period of chemical evolution when the dust was cold, as in theories of Galactic hot-core formation.

5.2.2. Models for COM Ice–Gas Synthesis. Given the importance of NH_3 for gaseous COM formation, the Magellanic Clouds offer a potential opportunity to test this scenario in a low-metallicity environment. In ref 159, it was emphasized that the sublimation of COM-containing ice mantles into the hot gas, not active formation *in situ*, as the possible source of Magellanic COMs. Post-sublimation gas-phase synthesis (see section 5.1.3) has not yet been studied in the context of the Magellanic Clouds, and here we report relevant model calculations as a first approximation.

The calculations were performed with the dynamical–chemical model of ref 132, but modified according to the simplest version of these models in which the physical conditions are fixed in time and the ices are injected instantaneously into the hot gas at $t = 0$ (cf. ref 108), as opposed to computing the physical and chemical evolution of the core (e.g., gravitational collapse, protostellar luminosity heating, time-dependent molecule desorption). Table 4 lists the assumed ice mantle compositions. These were obtained by scaling the ice abundances from Table 1 of ref 132 to the elemental depletions observed in the SMC and LMC clouds as listed in Table 1 of refs 155 ($f_{\text{LMC},i}$) and 156 ($f_{\text{SMC},i}$), respectively. The (C, O, N) scaling factors ($1/f$) are (0.41, 0.46, 0.21) for the LMC and (0.20, 0.22, 0.064) for the SMC; for each molecule listed in Table 4, we used the averaged $1/f$ of its corresponding elements to determine initial ice abundances in the LMC/SMC from their Galactic values used in ref 132. Typical hot-core physical conditions were assumed: $n_{\text{H}_2} = 5 \times 10^7 \text{ cm}^{-3}$, $T = 150 \text{ K}$, and a cosmic-ray ionization rate $\zeta = 3 \times 10^{-17} \text{ s}^{-1}$. The chemical network is as discussed in ref 132. Figure 14 shows COM chemical evolution in hot-core models applicable to the LMC and SMC. Generally, one can notice a decrease of all gas phase abundances by a factor of a few depending on the elemental depletion of C, N, and O in the two galaxies. However, the stronger N depletion relative to C and O (by a factor of 2 and 4 for the LMC and SMC, respectively) induces a more pronounced decrease of NH_3 relative to other ice species.

As reported in ref 132, a decrease of the injected ice mantle $\text{NH}_3/\text{CH}_3\text{OH}$ abundance ratio from ~ 1 decreases the production efficiency of COMs; for CH_3OCH_3 and HCOOCH_3 the Magellanic Cloud abundances are lower by a factor of 3 for the LMC and of 5 for the SMC. The NH_3 abundance is not observationally well-constrained in the LMC and SMC and is unknown in the N113 region. An ammonia abundance of $\sim 4 \times 10^{-10}$ was measured in N159W in the LMC,³⁶ and Figure 15 shows that systematically reducing the injected NH_3 abundance from ices dramatically lowers the COM abundances. However,

Table 4. Model Ice Mantle Compositions^a

molecule	LMC	SMC
H_2O	4.5×10^{-5}	2.2×10^{-5}
CO	1.7×10^{-5}	7.6×10^{-6}
CO_2	1.3×10^{-5}	6.0×10^{-6}
CH_4	2.1×10^{-6}	1.0×10^{-6}
NH_3	1.0×10^{-6}	3.2×10^{-7}
N_2	3.2×10^{-6}	1.0×10^{-6}
H_2CO	1.1×10^{-6}	5.0×10^{-7}
CH_3OH	3.2×10^{-6}	1.4×10^{-6}
HCOOH	6.4×10^{-7}	3.2×10^{-7}

^aAbundances are given relative to total density of hydrogen nuclei.

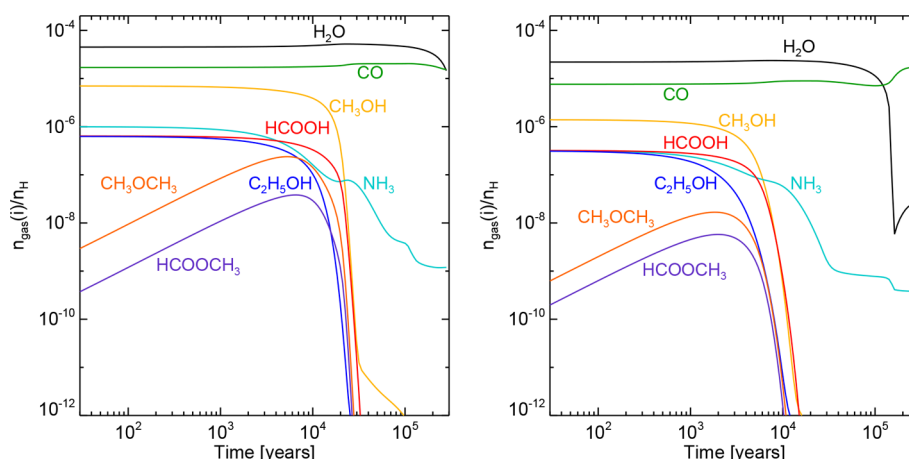


Figure 14. Chemical evolution in hot-core models of the LMC (left panel) and SMC (right panel). Ice mantles with the compositions of Table 4 are instantaneously injected into the gas at $t = 0$.

any decline in COMs below an NH_3 abundance of $\sim 10^{-8}$, down to the level measured in ref 36, is halted as electron dissociative recombinations come to dominate the loss of molecular ions. Although models of ice formation in the Magellanic Clouds do predict $\text{NH}_3/\text{H}_2\text{O}$ mantle fractions sufficiently large to allow efficient ion–molecule formation in the LMC (see section 5.2.1), NH_3 observations of N113 and other COM-containing regions are clearly required to validate the efficacy of this process.

The observed abundances of CH_3OCH_3 and HCOOCH_3 in the A1 and B3 hot cores of N113 (see Table 3) can be reproduced in the models of Figure 14, despite the lower elemental depletions. However, as in the case of Galactic hot-core models these do not occur at a time when the $\text{CH}_3\text{OCH}_3/\text{CH}_3\text{OH}$ and $\text{HCOOCH}_3/\text{CH}_3\text{OH}$ abundance ratios have their observed values (Figure 16). In the LMC, when the methanol abundance is $\sim 10^{-8}$, the observed $\text{CH}_3\text{OCH}_3/\text{CH}_3\text{OH}$ ratios in A1 (~ 0.1) and B3 (~ 0.2) are about an order of magnitude higher than the calculated values (~ 0.01); for $\text{HCOOCH}_3/\text{CH}_3\text{OH}$ the calculated value of (~ 0.003) is about a factor 20 too low.

In ref 159, the authors claimed a very good agreement with the abundances of ref 18 to within a factor of 5. However, calculated abundances and the observed abundances were presented as relative to total hydrogen density and molecular hydrogen density, respectively. Correcting the abundance comparison by the factor of 2 means that for CH_3OCH_3 in A1 and B3, the models overpredict the abundances by factors of 12–20; only the calculated abundances of CH_3OH and HCOOCH_3 in A1 agree to within a factor of 5.

When a detailed treatment of the collapse physics is included in hot-core chemistry models, a monotonic increase in the radial gas and dust temperatures occurs as a function of the increasing (accretion) luminosity of the protostar (e.g., ref 109). In the case of Galactic hot cores/corinos, ref 132 showed that molecular *recondensation* may be just as chemically important as molecular depletion onto dust in cold cores, and sublimation from them in hot cores. This can occur if the accretion onto the protostar is not monotonic but sporadic.¹⁶⁰ Once grains have been raised to a temperature of about 120 K or more, most of the ice mantle is removed and, as they cool to 50 K or lower in about 100 years, selective recondensation can occur due to the differing binding energies for physisorption. Production of organic molecules ensues in the brief post-sublimation period, as in the standard

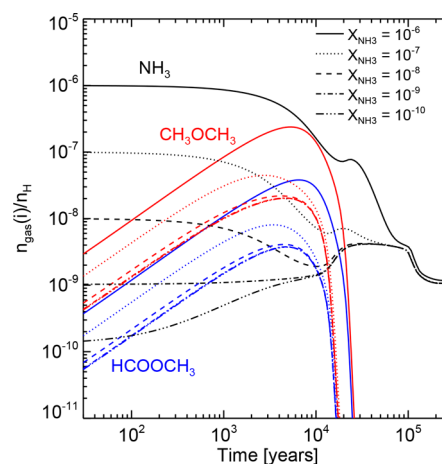


Figure 15. Evolution of CH_3OCH_3 and HCOOCH_3 abundances in the LMC model as a function of the NH_3 abundance sublimated from ices.

model, except that the products subsequently condense as ices. It was demonstrated in ref 132 that the observed large $\text{CH}_3\text{OCH}_3/\text{CH}_3\text{OH}$ and $\text{HCOOCH}_3/\text{CH}_3\text{OH}$ ratios could be reproduced due to the relatively higher binding energy of

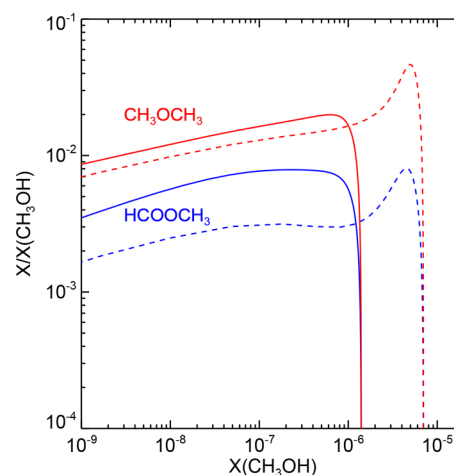


Figure 16. Evolution of the $\text{CH}_3\text{OCH}_3/\text{CH}_3\text{OH}$ and $\text{HCOOCH}_3/\text{CH}_3\text{OH}$ abundance ratios in the models of Figure 14 for the LMC (solid curves) and SMC (dashed curves).

CH₃OH. This may be a fundamental process for the organic chemistry of material near protostars, as between sublimation–recondensation events, there can be a mantle-driven gaseous chemistry leading to the dust grains being coated with the products as they cool. This scenario remains to be evaluated in the context of Magellanic Cloud hot cores.

6. DISCUSSION

Although single-dish observations provided the first detections of methanol in two bright regions in the LMC (N159 and N113), it was ALMA with its unprecedented angular resolution and sensitivity that has started and continue revolutionizing the field of complex organic chemistry in low-metallicity environments. To date, the sample of sources with COMs detection is very small and diverse. Only two *bona fide* hot cores with COMs are known in the Magellanic Clouds, both in the N113 star-forming region in the LMC (N113 A1 and B3).¹⁸ Another hot core in the LMC (ST11) was reported in ref 73, but no methanol or other COMs were detected. The detection of methanol was reported for two other sources, one in the LMC (N159W-S, section A.1) and one in the SMC (IRAS 01042-7215),¹⁹ but not in hot cores (“cold methanol”). Several sources in N113 (in addition to two hot cores) are associated with methanol, but due to a very low spectral resolution of the observations, a determination of their physical parameters based on the existing data is currently impossible. Table 5 summarizes the COM transitions detected in the Magellanic Clouds with ALMA.

No firm conclusions about complex organic chemistry under reduced metallicity conditions can be drawn based on the current sample of sources with the detection of COMs. However, some general trends are noticeable.

None of the sources with a COMs detection is associated with an infrared source: COMs are detected toward mm continuum sources in the vicinity of bright *Spitzer* YSOs. ST11 with no COMs detection but with evidence for hot-core chemistry is the only source associated with the infrared source. In fact, this is the brightest *Spitzer* YSO in the entire N144 H II region;⁵¹ higher resolution near-infrared observations reveal a cluster with one dominating source (see Figure 2), which likely has the largest contribution to the emission at longer wavelengths. Multiple mm continuum sources are detected toward all the other fields. The N113 B3 field is particularly interesting since it harbors sources at different evolutionary stages, including a hot core and ultracompact H II regions with younger sources distributed along a dense gas filament (see Figures 9 and ref 12). Several mm continuum sources, including one associated with the brightest CH₃OH peaks in the region, are also found along the filament in N159W-S (see Figures 4 and 5 and ref 76).

The detection of cold methanol in N159W-S and IRAS 01042-7215 P2/P3 is puzzling; however, similar results are being obtained in our Galaxy. In Galactic dark clouds, gas-phase methanol is found to have a clumpy distribution, often not following the density distribution traced by continuum and molecular tracers,¹⁶¹ and thus provides evidence of rapid ice desorption processes. This methanol tends to be cold, at excitation temperatures of 5–20 K, similar to what is observed in N159W-S and IRAS 01042-7215. In the Barnard 5 cloud in particular, a cold methanol clump with the CH₃OH abundance with respect to H₂ of $\sim 4 \times 10^{-8}$, offset from the IRAS sources, has proven to be a signpost of ice desorption—by the detection of first cold gas-phase water at abundances similar to that found in methanol¹⁶² and then other COMs like CH₃CHO and HCOOCH₃, likely formed by gas-phase chemistry following an

Table 5. COM Transitions Detected in the Magellanic Clouds with ALMA^a

species	transition	frequency (GHz)	E_U (K)	detection ^b	
LMC N113				A1	B3
CH ₃ OH, $\nu_t = 0$	5 _{1,4} –4 _{2,2} E	216.94560	55.87	+	+
CH ₃ OH, $\nu_t = 1$	6 _{1,5} –7 _{2,6} A [–]	217.299205	373.93	+	+
CH ₃ OH, $\nu_t = 0$	20 _{1,19} –20 _{0,20} E	217.88639	508.38	+	–
CH ₃ OH, $\nu_t = 0$	10 _{2,9} –9 _{3,6} A [–]	231.28110	165.35	+	+
CH ₃ OH, $\nu_t = 0$	10 _{2,8} –9 _{3,7} A ⁺	232.41859	165.40	+	+
CH ₃ OH, $\nu_t = 0$	18 _{3,16} –17 _{4,13} A ⁺	232.78350	446.53	+	+
CH ₃ OH, $\nu_t = 0^c$	2 _{–1,2} –1 _{–1,1} E	96.739362	12.54	+	+
	2 _{0,2} –1 _{0,1} A ⁺	96.741375	6.97		
	2 _{0,2} –1 _{0,1} E	96.744550	20.09		
	2 _{1,1} –1 _{1,0} E	96.755511	28.01		
HCOOCH ₃ , $\nu = 0$	18 _{2,16} –17 _{2,15} E	216.83020	105.68	+	–
HCOOCH ₃ , $\nu = 0$	18 _{2,16} –17 _{2,15} A	216.83889	105.67	+	–
HCOOCH ₃ , $\nu = 0$	20 _{1,20} –19 _{1,19} E	216.96476	111.50	+	+
HCOOCH ₃ , $\nu = 0$	20 _{1,20} –19 _{1,19} A	216.96590	111.48	+	+
HCOOCH ₃ , $\nu = 0$	20 _{0,20} –19 _{0,19} E	216.96625	111.50	+	+
HCOOCH ₃ , $\nu = 0$	20 _{0,20} –19 _{0,19} A	216.96742	111.48	+	+
CH ₃ OCH ₃	13 _{0,13} –12 _{1,12} EE	231.98782	80.92	+	+
LMC N159W-S				MMS-3 ^d	
CH ₃ OH, $\nu_t = 0$	5 _{0,5} –4 _{0,4} E	241.700219	47.93	+	
CH ₃ OH, $\nu_t = 0$	5 _{–1,5} –4 _{–1,4} E	241.767224	40.39	+	
CH ₃ OH, $\nu_t = 0$	5 _{0,5} –4 _{0,4} A ⁺	241.791431	34.82	+	
CH ₃ OH, $\nu_t = 0$	5 _{1,4} –4 _{1,3} E	241.879073	55.87	+	
CH ₃ OH, $\nu_t = 0^e$	5 _{–2,4} –4 _{–2,3} E	241.904152	60.72	+	
	5 _{2,3} –4 _{2,2} E	241.904645	57.07		
SMC IRAS 01042-7215				P2	P3
CH ₃ OH, $\nu_t = 0$	5 _{0,5} –4 _{0,4} A ⁺	241.791431	34.82	+	+
CH ₃ OH, $\nu_t = 0$	5 _{–1,5} –4 _{–1,4} E	241.767224	40.39	+	+
CH ₃ OH, $\nu_t = 0$	5 _{0,5} –4 _{0,4} E	241.700219	47.93	+	–
CH ₃ OH, $\nu_t = 0^e$	5 _{–2,4} –4 _{–2,3} E	241.904152	60.72	+	–
	5 _{2,3} –4 _{2,2} E	241.904645	57.07		

^aThe table uses the CDMS notation from the Splatalogue. See footnotes to Table 1 for details. ^bThe symbols in these columns indicate a detection (+), a tentative detection (+?), or a non-detection (–) of a given molecular line transition; ^cThe four transitions at ~ 96.7 GHz are blended; the spectral resolution of these observations, which were dedicated to the continuum detection, is ~ 50 km s^{–1}. In addition to hot cores A1 and B3, there are several other ~ 96.7 GHz CH₃OH peaks in N113 (see section 4.3). ^dThe two methanol peaks associated with MMS-3 where the largest number of CH₃OH lines are detected and the temperature fitting is the most reliable (see section 4.2.1). ^eThe CH₃OH lines at 241.904152 and 241.904645 GHz are blended.

ice desorption event.¹⁰² However, the low yield of COMs from ice desorption at cold temperatures is at most a few percent of methanol even at Galactic metallicities, thus consistent with non-detections of COMs toward N159W-S, IRAS 01042-7215 P2 and P3.

For IRAS 01042-7215, where the CH₃OH emission is detected toward two sources corresponding to the continuum peak, the authors of ref 19 discussed three possibilities for the nature of P2/P3 (their “east core”) where cold methanol was

detected: they suggested it can be either a massive starless core, an embedded high-mass YSO (or multiple YSOs) before the emergence of infrared emission, or a cluster of low-mass embedded YSOs.

Observations confirm that COMs can form in extragalactic environments. Formation pathways have been suggested that involve either grain–surface chemistry or gas-phase chemistry, or a combination of both. Theoretical models accounting for the physical conditions and metallicity of hot molecular cores in the Magellanic Clouds have been able to broadly account for the existing observations.

As cosmic metallicity is increasing with time, understanding interstellar chemistry in low metallicity environments also gives us insight into the chemistry of the past universe. The detection of COMs in the Magellanic Clouds has important implications for astrobiology. The metallicity of the LMC/SMC is similar to the mean metallicity of the interstellar medium during the epoch of peak star formation in the universe, thus the presence of COMs in these systems indicates that a similar prebiotic chemistry leading to the emergence of life, as it happened on Earth, is possible in low-metallicity systems in earlier epochs of the universe. According to one of the theories on the emergence of life on Earth, interstellar COMs (after incorporating into comets) might have been delivered to early Earth to provide important ingredients for the origin of life (e.g., refs 1, 89, and 163).

COMs more complex than CH₃OH are detected in the LMC toward hot cores which are associated with massive stars and therefore are short-lived; a detection of COMs does not have a direct relation to the origin of life at these locations. However, if COMs are detected toward hot cores, we can expect them to be present in hot corinos, which are associated with low-mass stars. The evolution of low-mass stars is long enough for life to emerge if favorable conditions exist.

7. FUTURE PROSPECTS

Systematic studies on YSOs in different environments in the LMC and SMC are needed to build a statistically significant sample of sources with COMs detections in the Magellanic Clouds that would allow us to draw reliable conclusions on the formation and evolution of COMs in reduced metallicity environments. Both the LMC and SMC samples will be important to get as wide a range of metallicities as possible. In the SMC, the metallicity is lower than in the LMC (as low as 0.1 Z_{\odot} in the SMC tail where star formation occurs in pockets; e.g., ref 164), and the formation and survival of COMs can be tested in an even harsher environment. Enlarging the sample in both galaxies is important to distinguishing between local environmental conditions in individual clouds and the more global effect of metallicity.

Reliable determination of Magellanic Clouds hot cores' physical and chemical properties and a comparison between the two clouds and the Galaxy are of paramount importance to understand the impact of metallicity on complex organic chemistry. High-resolution and high-sensitivity observations of known hot cores in the Magellanic Clouds as their number starts increasing are a natural next step in reaching this goal. This direction of research involves chemical modeling of hot cores to understand their chemical evolution.

ALMA programs are underway targeting tens of YSOs identified by *Spitzer* and *Herschel*, both specifically designed to search for COMs and those with different science goals, but covering frequency ranges where COMs can be detected

(serendipitous detections as in N113). ALMA's broad spectral windows allow the simultaneous observation of many spectral lines, with the spectral setup covering the most important molecules.

What new COMs await discovery in the Magellanic Clouds? Chemical models of the LMC have not been successful (to within an order of magnitude) in accounting for the observed presence of dimethyl ether in the LMC (see section 5.2.2) and so may not be reliable indicators for new molecules. At present, taking the inventory of well-studied Galactic hot cores may provide the best guidelines for future searches. Molecules that could be expected to be present include acetaldehyde, ethanol, ethyl cyanide, isocyanic acid, and formamide.

NASA's James Webb Space Telescope (*JWST*; scheduled to launch in 2021) near- (0.6–5.3 μm ; the Near-Infrared Spectrograph (NIRSpec) instrument) to mid-infrared (4.9–28.8 μm ; the Mid-Infrared Instrument (MIRI)) observations will enable studies of the solid-phase material in different Galactic and extragalactic environments. The high sensitivity and angular resolution of *JWST* will enable detailed studies of hot cores in the Magellanic Clouds on ~ 0.04 pc scales in the near-infrared, without contamination from the surrounding regions. It will be possible to do an inventory of simple (e.g., H₂O, CO₂, CO) and complex (CH₃OH and beyond, including molecules of prebiotic significance) ices in the low-metallicity environments in the Magellanic Clouds. For example, in the 5–8 μm range (MIRI), COMs such as ethylene glycol, glycol-aldehyde, methyl formate, dimethyl ether (the latter two already detected in N113 A1/B3 in the gas phase with ALMA), and others can be detected.¹⁶⁵ Laboratory experiments are underway predicting which COMs can be detected at shorter wavelengths covered by NIRSpec. Such studies will provide information on differences in the chemical complexity of hot cores in different environments.

■ APPENDIX A: TECHNICAL DETAILS ON UNPUBLISHED OBSERVATIONS REPORTED IN THIS PAPER

The ALMA and VLT/KMOS data presented in section 4.2.1 for N159W-S have not been published in literature yet. Below we summarize technical details of these observations.

A.1. ALMA

N159W-S was observed with ALMA (Atacama Large Millimeter/submillimeter Array; ALMA Partnership et al., 2015) during its Cycle 4 in October 2016 as part of project number 2016.1.00308.S. We used the main array (i.e., 12-m antennas) consisting of 40 antennas. The phase center was set to RA (J2000) = 05^h39^m41^s, Dec (J2000) = 69°46'11". The ALMA correlator was configured to cover specific frequency ranges within the Band 6 of ALMA. Four broad spectral windows (with a bandwidth of 1875 MHz each) centered at frequencies 242.4, 244.8, 257.85, and 259.7 GHz were tuned at the frequencies of specific molecular transitions of dense gas, shock/hot core tracers (e.g., CS, SO₂, CH₃OH, and SiO). The ALMA data were calibrated using the ALMA calibration pipeline available in CASA version 5.5.1. Flux calibration was obtained through observations of the bright quasar J0519-4546. The gains were calibrated by interleaved observations of the quasar J0601-7036. The bandpass response was obtained by observing the bright quasar J0635-7516. After the calibration was applied, the line-free channels of the broad spectral windows were identified and used to create the continuum images. The images were made

using the CASA task TCLEAN with a robust parameter of Briggs equal to 0.5 as compromise between resolution and sensitivity. The resulting images were restored with a synthesized beam of $0''.22 \times 0''.12$. Sensitivity of $1.4 \text{ mJy beam}^{-1}$ was achieved in the data cube covering the CH_3OH lines.

A.2. VLT/KMOS

N159W-S was observed with VLT/KMOS (Very Large Telescope/K-band Multi-Object Spectrograph) under program 0101.C-0856(A) using the H+K grating with a spectral resolving power of 2000. The observations were carried out using a standard nod-to-sky procedure with an integration time of 150 s, four DITs, and three dither positions, yielding a total on-source integration time of 1800 s. Telluric absorption correction, response curve correction, and absolute flux calibration were carried out using observations of telluric standard stars using three IFUs. The data were reduced with the standard VLT/KMOS pipeline using the ESOREFLEX data reduction package. The K-band continuum image is produced by integrating over a third-order polynomial fit to the data for every spatial pixel (spaxel) over the spectral range $2.028\text{--}2.290 \mu\text{m}$. The Br γ and H $_2$ line emission images are produced by fitting a Gaussian profile to the emission lines at every position in the image.

AUTHOR INFORMATION

Corresponding Author

*E-mail: marta.m.sewilo@nasa.gov.

ORCID

Marta Sewilo: 0000-0003-2248-6032

Jacco Th. van Loon: 0000-0002-1272-3017

Notes

The authors declare no competing financial interest.

ACKNOWLEDGMENTS

We thank Dr. Kazuki Tokuda for providing the ALMA 1.3 mm continuum image of N159W-S and Dr. Julia Roman-Duval for providing the CH_3OH $\sim 96.7 \text{ GHz}$ image of N113. We also thank Dr. Gerard Testor for providing the VLT/NACO near-infrared images that were used to improve astrometry of the VLT/KMOS images. The work of M.S. was supported by NASA under award number 80GSFC17M0002. The work of S.B.C. was supported by the NASA Astrobiology Institute through the Goddard Center for Astrobiology. P.S. acknowledges support from the University of Cologne, Collaborative Research Centre 956, sub-project C3, funded by the Deutsche Forschungsgemeinschaft (DFG), project ID 18401886, and Verbundforschung Astrophysics, Project 05A17PK1, funded by BMBF (German Ministry of Science and Education). V.T. acknowledges financial support from the European Union's Horizon 2020 research and innovation program under Marie Skłodowska-Curie grant agreement no. 664931. E.W. received funding from the Swedish National Space Agency, grants dnr 98/14 and dnr 246/16. The work of J.W. was supported by Sonderforschungsbereich SFB 881 "The Milky Way System" (subproject B2) of the German Research Foundation (DFG). The work of S.Z. and T.O. was supported by NAOJ ALMA Scientific Research Grant Number 2016-03B. The work of T.O. was also supported by JSPS KAKENHI (Grant Nos. 22244014, 26247026, and 18H05440). The work of A.K. was supported by JSPS KAKENHI (Grant No. 23403001). The authors acknowledge financial support from their home institutions.

REFERENCES

- (1) Ehrenfreund, P.; Charnley, S. B. Organic Molecules in the Interstellar Medium, Comets, and Meteorites: A Voyage from Dark Clouds to the Early Earth. *Annu. Rev. Astron. Astrophys.* **2000**, *38*, 427–483.
- (2) Pietrzyński, G.; et al. An eclipsing-binary distance to the Large Magellanic Cloud accurate to two per cent. *Nature* **2013**, *495*, 76–79.
- (3) Graczyk, D.; Pietrzyński, G.; Thompson, I. B.; Gieren, W.; Pilecki, B.; Konorski, P.; Udalski, A.; Soszyński, I.; Villanova, S.; Górski, M.; Suchomska, K.; Karczmarek, P.; Kudritzki, R.-P.; Bresolin, F.; Gallenne, A. The Araucaria Project. The Distance to the Small Magellanic Cloud from Late-type Eclipsing Binaries. *Astrophys. J.* **2014**, *780*, 59.
- (4) Asplund, M.; Grevesse, N.; Sauval, A. J.; Scott, P. The Chemical Composition of the Sun. *Annu. Rev. Astron. Astrophys.* **2009**, *47*, 481–522.
- (5) Russell, S. C.; Dopita, M. A. Abundances of the heavy elements in the Magellanic Clouds. III - Interpretation of results. *Astrophys. J.* **1992**, *384*, 508–522.
- (6) Westerlund, B. E. *The Magellanic Clouds*; Cambridge University Press: Cambridge, UK, 1997.
- (7) Dufour, R. J. The composition of H II regions in the Magellanic Clouds. *Structure and Evolution of the Magellanic Clouds*, Symposium 108; International Astronomical Union, 1984; pp 353–360.
- (8) Koornneef, J. Gas-to-dust ratios in the Magellanic Clouds. *Structure and Evolution of the Magellanic Clouds*, Symposium 108; International Astronomical Union, 1984; pp 333–339.
- (9) Roman-Duval, J.; et al. Dust and Gas in the Magellanic Clouds from the HERITAGE Herschel Key Project. II. Gas-to-dust Ratio Variations across Interstellar Medium Phases. *Astrophys. J.* **2014**, *797*, 86.
- (10) van Loon, J. T.; Oliveira, J. M.; Gordon, K. D.; Sloan, G. C.; Engelbracht, C. W. A Spitzer Space Telescope Far-infrared Spectral Atlas of Compact Sources in the Magellanic Clouds. II. The Small Magellanic Cloud. *Astron. J.* **2010**, *139*, 1553–1565.
- (11) Oliveira, J. M.; van Loon, J. T.; Sloan, G. C.; Indebetouw, R.; Kemper, F.; Tielens, A. G. G. M.; Simon, J. D.; Woods, P. M.; Meixner, M. Ice chemistry in massive young stellar objects: the role of metallicity. *MNRAS* **2011**, *411*, L36–L40.
- (12) Browning, M. K.; Tumlinson, J.; Shull, J. M. Inferring Physical Conditions in Interstellar Clouds of H $_2$. *Astrophys. J.* **2003**, *582*, 810–822.
- (13) Abdo, A. A.; et al. Observations of the Large Magellanic Cloud with Fermi. *Astron. Astrophys.* **2010**, *512*, A7.
- (14) Knödseder, J. GeV Gamma-Ray Emission from Normal and Starburst Galaxies. Cosmic Rays in Star-Forming Environments. *Astrophys. Space Sci. Proc.* **2013**, *34*, 169.
- (15) Pei, Y. C.; Fall, S. M.; Hauser, M. G. Cosmic Histories of Stars, Gas, Heavy Elements, and Dust in Galaxies. *Astrophys. J.* **1999**, *522*, 604–626.
- (16) Heikkilä, A.; Johansson, L. E. B.; Olofsson, H. Molecular abundance variations in the Magellanic Clouds. *Astron. Astrophys.* **1999**, *344*, 817–847.
- (17) Wang, M.; Chin, Y.-N.; Henkel, C.; Whiteoak, J. B.; Cunningham, M. Abundances and Isotope Ratios in the Magellanic Clouds: The Star-Forming Environment of N 113. *Astrophys. J.* **2009**, *690*, 580–597.
- (18) Sewilo, M.; Indebetouw, R.; Charnley, S. B.; Zahorecz, S.; Oliveira, J. M.; van Loon, J. T.; Ward, J. L.; Chen, C.-H. R.; Wiseman, J.; Fukui, Y.; Kawamura, A.; Meixner, M.; Onishi, T.; Schilke, P. The Detection of Hot Cores and Complex Organic Molecules in the Large Magellanic Cloud. *Astrophys. J., Lett.* **2018**, *853*, L19.
- (19) Shimonishi, T.; Watanabe, Y.; Nishimura, Y.; Aikawa, Y.; Yamamoto, S.; Onaka, T.; Sakai, N.; Kawamura, A. A Multiline Study of a High-mass Young Stellar Object in the Small Magellanic Cloud with ALMA: The Detection of Methanol Gas at 0.2 Solar Metallicity. *Astrophys. J.* **2018**, *862*, 102.
- (20) McGuire, B. A. 2018 Census of Interstellar, Circumstellar, Extragalactic, Protoplanetary Disk, and Exoplanetary Molecules. *Astrophys. J., Suppl. Ser.* **2018**, *239*, 17.

- (21) Meixner, M.; et al. The HERSCHEL Inventory of The Agents of Galaxy Evolution in the Magellanic Clouds, a Herschel Open Time Key Program. *Astron. J.* **2013**, *146*, 62.
- (22) Cohen, R. S.; Dame, T. M.; Garay, G.; Montani, J.; Rubio, M.; Thaddeus, P. A complete CO survey of the Large Magellanic Cloud. *Astrophys. J.* **1988**, *331*, L95–L99.
- (23) Rubio, M.; Garay, G.; Montani, J.; Thaddeus, P. A (C-12)O survey of the Small Magellanic Cloud. *Astrophys. J.* **1991**, *368*, 173–177.
- (24) Fukui, Y.; et al. First Results of a CO Survey of the Large Magellanic Cloud with NANTEN; Giant Molecular Clouds as Formation Sites of Populous Clusters. *Publ. Astron. Soc. Jpn.* **1999**, *51*, 745–749.
- (25) Mizuno, N.; Rubio, M.; Mizuno, A.; Yamaguchi, R.; Onishi, T.; Fukui, Y. First Results of a CO Survey of the Small Magellanic Cloud with NANTEN. *Publ. Astron. Soc. Jpn.* **2001**, *53*, L45–L49.
- (26) Fukui, Y.; Kawamura, A.; Minamidani, T.; Mizuno, Y.; Kanai, Y.; Mizuno, N.; Onishi, T.; Yonekura, Y.; Mizuno, A.; Ogawa, H.; Rubio, M. The Second Survey of the Molecular Clouds in the Large Magellanic Cloud by NANTEN. I. Catalog of Molecular Clouds. *Astrophys. J., Suppl. Ser.* **2008**, *178*, 56–70.
- (27) Wong, T.; et al. The Magellanic Mopra Assessment (MAGMA). I. The Molecular Cloud Population of the Large Magellanic Cloud. *Astrophys. J., Suppl. Ser.* **2011**, *197*, 16.
- (28) Israel, F. P.; Johansson, L. E. B.; Lequeux, J.; Booth, R. S.; Nyman, L. A.; Crane, P.; Rubio, M.; de Graauw, T.; Kutner, M. L.; Gredel, R.; Boulanger, F.; Garay, G.; Westerlund, B. Results of the ESO/SEST Key Programme on CO/ in the Magellanic Clouds - Part One - a Survey of CO/ in the Large Magellanic Cloud and the Small Magellanic Cloud. *Astron. Astrophys.* **1993**, *27*, 25.
- (29) Israel, F. P.; Johansson, L. E. B.; Rubio, M.; Garay, G.; de Graauw, T.; Booth, R. S.; Boulanger, F.; Kutner, M. L.; Lequeux, J.; Nyman, L. A. Results of the ESO-SEST Key Programme on CO in the Magellanic Clouds. X. CO emission from star formation regions in LMC and SMC. *Astron. Astrophys.* **2003**, *406*, 817–828.
- (30) Heikkilä, A.; Johansson, L. E. B.; Olofsson, H. The C¹⁸O/C¹⁷O ratio in the Large Magellanic Cloud. *Astron. Astrophys.* **1999**, *332*, 493–502.
- (31) Johansson, L. E. B.; Olofsson, H.; Hjalmarson, A.; Gredel, R.; Black, J. H. Interstellar molecules in the Large Magellanic Cloud. *Astron. Astrophys.* **1994**, *291*, 89–105.
- (32) Chin, Y.-N.; Henkel, C.; Whiteoak, J. B.; Millar, T. J.; Hunt, M. R.; Lemme, C. Molecular abundances in the Magellanic Clouds. I. A multiline study of five cloud cores. *Astron. Astrophys.* **1997**, *317*, 548–562.
- (33) Chin, Y.-N.; Henkel, C.; Millar, T. J.; Whiteoak, J. B.; Marx-Zimmer, M. Molecular abundances in the Magellanic Clouds. III. LIRS36, a star-forming region in the Small Magellanic Cloud. *Astron. Astrophys.* **1998**, *330*, 901–909.
- (34) Wong, T.; Whiteoak, J. B.; Ott, J.; Chin, Y.-n.; Cunningham, M. R. Synthesis Imaging of Dense Molecular Gas in the N113 H II Region of the Large Magellanic Cloud. *Astrophys. J.* **2006**, *649*, 224–234.
- (35) Seale, J. P.; Looney, L. W.; Wong, T.; Ott, J.; Klein, U.; Pineda, J. L. The Life and Death of Dense Molecular Clumps in the Large Magellanic Cloud. *Astrophys. J.* **2012**, *751*, 42.
- (36) Ott, J.; Henkel, C.; Staveley-Smith, L.; Weiß, A. First Detection of Ammonia in the Large Magellanic Cloud: The Kinetic Temperature of Dense Molecular Cores in N 159 W. *Astrophys. J.* **2010**, *710*, 105–111.
- (37) Nishimura, Y.; Shimonishi, T.; Watanabe, Y.; Sakai, N.; Aikawa, Y.; Kawamura, A.; Yamamoto, S. Spectral Line Survey toward Molecular Clouds in the Large Magellanic Cloud. *Astrophys. J.* **2016**, *818*, 161.
- (38) Green, J. A.; et al. Multibeam maser survey of methanol and excited OH in the Magellanic Clouds: new detections and maser abundance estimates. *Mon. Not. R. Astron. Soc.* **2008**, *385*, 948–956.
- (39) Sinclair, M. W.; Carrad, G. J.; Caswell, J. L.; Norris, R. P.; Whiteoak, J. B. A methanol maser in the Large Magellanic Cloud. *Mon. Not. R. Astron. Soc.* **1992**, *256*, 33P.
- (40) Ellingsen, S. P.; Whiteoak, J. B.; Norris, R. P.; Caswell, J. L.; Vaile, R. A. A Search for Methanol Masers in the Magellanic Clouds. *Mon. Not. R. Astron. Soc.* **1994**, *269*, 1019.
- (41) Beasley, A. J.; Ellingsen, S. P.; Claussen, M. J.; Wilcots, E. A. Methanol Maser Survey of IRAS-selected Regions in the Magellanic Clouds. *Astrophys. J.* **1996**, *459*, 600.
- (42) Ellingsen, S. P.; Breen, S. L.; Caswell, J. L.; Quinn, L. J.; Fuller, G. A. Masers associated with high-mass star formation regions in the Large Magellanic Cloud. *Mon. Not. R. Astron. Soc.* **2010**, *404*, 779–791.
- (43) Werner, M. W.; et al. The Spitzer Space Telescope Mission. *Astrophys. J., Suppl. Ser.* **2004**, *154*, 1–9.
- (44) Pilbratt, G. L.; Riedinger, J. R.; Passvogel, T.; Crone, G.; Doyle, D.; Gageur, U.; Heras, A. M.; Jewell, C.; Metcalfe, L.; Ott, S.; Schmidt, M. Herschel Space Observatory. An ESA facility for far-infrared and submillimetre astronomy. *Astron. Astrophys.* **2010**, *518*, L1.
- (45) Meixner, M.; et al. Spitzer Survey of the Large Magellanic Cloud: Surveying the Agents of a Galaxy's Evolution (SAGE). I. Overview and Initial Results. *Astron. J.* **2006**, *132*, 2268–2288.
- (46) Gordon, K. D.; et al. Surveying the Agents of Galaxy Evolution in the Tidally Stripped, Low Metallicity Small Magellanic Cloud (SAGE-SMC). I. Overview. *Astron. J.* **2011**, *142*, 102.
- (47) Whitney, B. A.; et al. Spitzer Space Survey of the Large Magellanic Cloud. III. Star Formation and ~1000 New Candidate Young Stellar Objects. *Astron. J.* **2008**, *136*, 18–43.
- (48) Gruendl, R. A.; Chu, Y. High- and Intermediate-Mass Young Stellar Objects in the Large Magellanic Cloud. *Astrophys. J., Suppl. Ser.* **2009**, *184*, 172–197.
- (49) Chen, C.-H. R.; Indebetouw, R.; Chu, Y.-H.; Gruendl, R. A.; Testor, G.; Heitsch, F.; Seale, J. P.; Meixner, M.; Sewilo, M. Spitzer View of Young Massive Stars in the Large Magellanic Cloud H II Complexes. II. N 159. *Astrophys. J.* **2010**, *721*, 1206–1232.
- (50) Romita, K. A.; Carlson, L. R.; Meixner, M.; Sewilo, M.; Whitney, B.; Babler, B.; Indebetouw, R.; Hora, J. L.; Meade, M.; Shiao, B. Young Stellar Objects in the Large Magellanic Cloud Star-forming Region N206. *Astrophys. J.* **2010**, *721*, 357–368.
- (51) Carlson, L. R.; Sewilo, M.; Meixner, M.; Romita, K. A.; Lawton, B. Identifying young stellar objects in nine Large Magellanic Cloud star-forming regions. *Astron. Astrophys.* **2012**, *542*, A66.
- (52) Sewilo, M.; et al. Surveying the Agents of Galaxy Evolution in the Tidally Stripped, Low Metallicity Small Magellanic Cloud (SAGE-SMC). III. Young Stellar Objects. *Astrophys. J.* **2013**, *778*, 15.
- (53) Sewilo, M.; et al. The youngest massive protostars in the Large Magellanic Cloud. *Astron. Astrophys.* **2010**, *518*, L73.
- (54) Seale, J. P.; et al. Herschel Key Program Heritage: a Far-Infrared Source Catalog for the Magellanic Clouds. *AJ* **2014**, *148*, 124.
- (55) Ita, Y.; et al. AKARI IRC Survey of the Large Magellanic Cloud: Outline of the Survey and Initial Results. *Publ. Astron. Soc. Jpn.* **2008**, *60*, S435–S451.
- (56) Kato, D.; Ita, Y.; Onaka, T.; Tanabé, T.; Shimonishi, T.; Sakon, I.; Kaneda, H.; Kawamura, A.; Wada, T.; Usui, F.; Koo, B.-C.; Matsuura, M.; Takahashi, H. AKARI Infrared Camera Survey of the Large Magellanic Cloud. I. Point-source Catalog. *Astron. J.* **2012**, *144*, 179.
- (57) Shimonishi, T.; Onaka, T.; Kato, D.; Sakon, I.; Ita, Y.; Kawamura, A.; Kaneda, H. AKARI Infrared Camera Survey of the Large Magellanic Cloud. II. The Near-infrared Spectroscopic Catalog. *Astron. J.* **2013**, *145*, 32.
- (58) Oliveira, J. M.; van Loon, J. T.; Chen, C.-H. R.; Tielens, A. G. G. M.; Sloan, G. C.; Woods, P. M.; Kemper, F.; Indebetouw, R.; Gordon, K. D.; Boyer, M. L.; Shiao, B.; Madden, S.; Speck, A. K.; Meixner, M.; Marengo, M. Ice Chemistry in Embedded Young Stellar Objects in the Large Magellanic Cloud. *Astrophys. J.* **2009**, *707*, 1269–1295.
- (59) Oliveira, J. M.; van Loon, J. T.; Sloan, G. C.; Sewilo, M.; Kraemer, K. E.; Wood, P. R.; Indebetouw, R.; Filipović, M. D.; Crawford, E. J.; Wong, G. F.; Hora, J. L.; Meixner, M.; Robitaille, T. P.; Shiao, B.; Simon, J. D. Early-stage young stellar objects in the Small Magellanic Cloud. *Mon. Not. R. Astron. Soc.* **2013**, *428*, 3001–3033.
- (60) Seale, J. P.; Looney, L. W.; Chen, C.-H. R.; Chu, Y.-H.; Gruendl, R. A. The Evolution of Massive Young Stellar Objects in the Large

Magellanic Cloud. II. Thermal Processing of Circumstellar Ices. *Astrophys. J.* **2011**, 727, 36.

(61) Shimonishi, T.; Onaka, T.; Kato, D.; Sakon, I.; Ita, Y.; Kawamura, A.; Kaneda, H. AKARI Near-Infrared Spectroscopy: Detection of H₂O and CO₂ Ices toward Young Stellar Objects in the Large Magellanic Cloud. *Astrophys. J.* **2008**, 686, L99.

(62) Shimonishi, T.; Onaka, T.; Kato, D.; Sakon, I.; Ita, Y.; Kawamura, A.; Kaneda, H. Spectroscopic observations of ices around embedded young stellar objects in the Large Magellanic Cloud with AKARI. *Astron. Astrophys.* **2010**, 514, A12.

(63) van Dishoeck, E. F. Astrochemistry of dust, ice and gas: introduction and overview. *Faraday Discuss.* **2014**, 168, 9.

(64) Whittet, D. C. B.; Bode, M. F.; Longmore, A. J.; Adamson, A. J.; McFadzean, A. D.; Aitken, D. K.; Roche, P. F. Infrared spectroscopy of dust in the Taurus dark clouds - Ice and silicates. *Mon. Not. R. Astron. Soc.* **1988**, 233, 321–336.

(65) Pontoppidan, K. M.; Salyk, C.; Bergin, E. A.; Brittain, S.; Marty, B.; Mousis, O.; Öberg, K. I. Volatiles in Protoplanetary Disks. *Protostars and Planets VI* **2014**, 363–385.

(66) Shimonishi, T.; Dartois, E.; Onaka, T.; Boulanger, F. VLT/ISAAC infrared spectroscopy of embedded high-mass YSOs in the Large Magellanic Cloud: Methanol and the 3.47 μ m band. *Astron. Astrophys.* **2016**, 585, A107.

(67) Bernard-Salas, J.; Peeters, E.; Sloan, G. C.; Cami, J.; Guiles, S.; Houck, J. R. The Spitzer IRS spectrum of SMP LMC 11. *Astrophys. J.* **2006**, 652, L29–L32.

(68) Tielens, A. G. G. M. Interstellar polycyclic aromatic hydrocarbon molecules. *Annu. Rev. Astron. Astrophys.* **2008**, 46, 289–337.

(69) Malek, S. E.; Cami, J.; Bernard-Salas, J. The Rich Circumstellar Chemistry of SMP LMC 11. *Astrophys. J.* **2012**, 744, 16.

(70) Cernicharo, J.; Heras, A. M.; Tielens, A. G. G. M.; Pardo, J. R.; Herpin, F.; Guélin, M.; Waters, L. B. F. M. Infrared Space Observatory's Discovery of C₄H₂, C₆H₂, and Benzene in CRL 618. *Astrophys. J.* **2001**, 546, L123–L126.

(71) Jones, O. C.; et al. The SAGE-Spec Spitzer Legacy program: the life-cycle of dust and gas in the Large Magellanic Cloud. Point source classification - III. *Mon. Not. R. Astron. Soc.* **2017**, 470, 3250–3282.

(72) Seale, J. P.; Looney, L. W.; Chu, Y.-H.; Gruendl, R. A.; Brandl, B.; Chen, C.-H. R.; Brandner, W.; Blake, G. A. The Evolution Of Massive Young Stellar Objects in the Large Magellanic Cloud. I. Identification and Spectral Classification. *Astrophys. J.* **2009**, 699, 150–167.

(73) Shimonishi, T.; Onaka, T.; Kawamura, A.; Aikawa, Y. The Detection of a Hot Molecular Core in the Large Magellanic Cloud with ALMA. *Astrophys. J.* **2016**, 827, L4.

(74) Kato, D.; et al. The IRSF Magellanic Clouds Point Source Catalog. *Publ. Astron. Soc. Jpn.* **2007**, 59, 615–641.

(75) Smith, R. C. MCELS Team, The UM/CTIO Magellanic Cloud emission-line survey. *Publ. Astron. Soc. Aust.* **1998**, 15, 163–64.

(76) Tokuda, K.; et al. An ALMA view of molecular filaments in the Large Magellanic Cloud II: An early stage of high-mass star formation embedded at colliding clouds in N159W-South. *arXiv e-prints* **2018**, arXiv:1811.04400 [astro-ph.GA]. <https://arxiv.org/abs/1811.04400>.

(77) Fukui, Y.; et al. High-mass Star Formation Triggered by Collision between CO Filaments in N159 West in the Large Magellanic Cloud. *Astrophys. J., Lett.* **2015**, 807, L4.

(78) Testor, G.; Lemaire, J. L.; Field, D.; Diana, S. VLT/NACO near-infrared imaging and spectroscopy of N159A in the LMC HII complex N159. *Astron. Astrophys.* **2006**, 453, S17–S24.

(79) van Loon, J. T.; Cohen, M.; Oliveira, J. M.; Matsuura, M.; McDonald, I.; Sloan, G. C.; Wood, P. R.; Zijlstra, A. A. Molecules and dust production in the Magellanic Clouds. *Astron. Astrophys.* **2008**, 487, 1055–1073.

(80) Ward, J. L.; Oliveira, J. M.; van Loon, J. T.; Sewilo, M. K- band integral field spectroscopy and optical spectroscopy of massive young stellar objects in the Small Magellanic Cloud. *Mon. Not. R. Astron. Soc.* **2017**, 464, 1512–1552.

(81) Shull, J. M.; Hollenbach, D. J. H₂ cooling, dissociation, and infrared emission in shocked molecular clouds. *Astrophys. J.* **1978**, 220, 525–537.

(82) Tielens, A. G. G. M. *The Physics and Chemistry of the Interstellar Medium*; Cambridge University Press: Cambridge, UK, 2005.

(83) Sakai, T.; Sakai, N.; Hirota, T.; Yamamoto, S. A Survey of Molecular Lines Toward Massive Clumps in Early Evolutionary Stages of High-mass Star Formation. *Astrophys. J.* **2010**, 714, 1658–1671.

(84) Oliveira, J. M.; van Loon, J. T.; Stanimirović, S.; Zijlstra, A. A. Massive young stellar objects in the Large Magellanic Cloud: water masers and ESO-VLT 3–4 μ m spectroscopy. *Mon. Not. R. Astron. Soc.* **2006**, 372, 1509–1524.

(85) Whiteoak, J. B.; Gardner, F. F. Observations of H₂O masers in nearby galaxies. *Mon. Not. R. Astron. Soc.* **1986**, 222, 513–523.

(86) Lazendic, J. S.; Whiteoak, J. B.; Klammer, I.; Harbison, P. D.; Kuiper, T. B. H. Accurate positions of H₂ O masers in the Large Magellanic Cloud. *Mon. Not. R. Astron. Soc.* **2002**, 331, 969–974.

(87) Ward, J. L.; Oliveira, J. M.; van Loon, J. T.; Sewilo, M. Integral field spectroscopy of massive young stellar objects in the N113 H II region in the Large Magellanic Cloud. *Mon. Not. R. Astron. Soc.* **2016**, 455, 2345–2362.

(88) Fontani, F.; Palau, A.; Caselli, P.; Sánchez-Monge, Á.; Butler, M. J.; Tan, J. C.; Jiménez-Serra, I.; Busquet, G.; Leurini, S.; Audard, M. Deuteration as an evolutionary tracer in massive-star formation. *Astron. Astrophys.* **2011**, 529, L7.

(89) Caselli, P.; Ceccarelli, C. Our astrochemical heritage. *Astron. Astrophys. Rev.* **2012**, 20, 56.

(90) Albertsson, T.; Semenov, D. A.; Vasyunin, A. I.; Henning, T.; Herbst, E. New Extended Deuterium Fractionation Model: Assessment at Dense ISM Conditions and Sensitivity Analysis. *Astrophys. J., Suppl. Ser.* **2013**, 207, 27.

(91) Gerner, T.; Shirley, Y. L.; Beuther, H.; Semenov, D.; Linz, H.; Albertsson, T.; Henning, T. Chemical evolution in the early phases of massive star formation. II. Deuteration. *Astron. Astrophys.* **2015**, 579, A80.

(92) Mookerjee, B.; Casper, E.; Mundy, L. G.; Looney, L. W. Kinematics and Chemistry of the Hot Molecular Core in G34.26 + 0.15 at High Resolution. *Astrophys. J.* **2007**, 659, 447–458.

(93) Bisschop, S. E.; Jørgensen, J. K.; van Dishoeck, E. F.; de Wachter, E. B. M. Testing grain-surface chemistry in massive hot-core regions. *Astron. Astrophys.* **2007**, 465, 913–929.

(94) Kurtz, S.; Cesaroni, R.; Churchwell, E.; Hofner, P.; Walmsley, C. M. Hot Molecular Cores and the Earliest Phases of High-Mass Star Formation. *Protostars and Planets IV*; University of Arizona Press, 2000; pp 299–326.

(95) Herbst, E.; van Dishoeck, E. F. Complex Organic Interstellar Molecules. *Annu. Rev. Astron. Astrophys.* **2009**, 47, 427–480.

(96) Ohishi, M.; Irvine, W. M.; Kaifu, N. Molecular Abundance Variations among and Within Cold, Dark Molecular Clouds. *Astrochemistry of Cosmic Phenomena* **1992**, 150, 171.

(97) Widicus Weaver, S. L.; Laas, J. C.; Zou, L.; Kroll, J. A.; Rad, M. L.; Hays, B. M.; Sanders, J. L.; Lis, D. C.; Cross, T. N.; Wehres, N.; McGuire, B. A.; Sumner, M. C. Deep, Broadband Spectral Line Surveys of Molecule-rich Interstellar Clouds. *Astrophys. J., Suppl. Ser.* **2017**, 232, 3.

(98) Bacmann, A.; Taquet, V.; Faure, A.; Kahane, C.; Ceccarelli, C. Detection of complex organic molecules in a prestellar core: a new challenge for astrochemical models. *Astron. Astrophys.* **2012**, 541, L12.

(99) Cernicharo, J.; Marcelino, N.; Roueff, E.; Gerin, M.; Jiménez-Escobar, A.; Muñoz Caro, G. M. Discovery of the Methoxy Radical, CH₃O, toward B1: Dust Grain and Gas-phase Chemistry in Cold Dark Clouds. *Astrophys. J., Lett.* **2012**, 759, L43.

(100) Vastel, C.; Ceccarelli, C.; Lefloch, B.; Bachiller, R. The Origin of Complex Organic Molecules in Prestellar Cores. *Astrophys. J., Lett.* **2014**, 795, L2.

(101) Jiménez-Serra, I.; Vasyunin, A. I.; Caselli, P.; Marcelino, N.; Billot, N.; Viti, S.; Testi, L.; Vastel, C.; Lefloch, B.; Bachiller, R. The Spatial Distribution of Complex Organic Molecules in the L1544 Prestellar Core. *Astrophys. J., Lett.* **2016**, 830, L6.

(102) Taquet, V.; Wiström, E. S.; Charnley, S. B.; Faure, A.; López-Sepulcre, A.; Persson, C. M. Chemical complexity induced by efficient

ice evaporation in the Barnard 5 molecular cloud. *Astron. Astrophys.* **2017**, 607, A20.

(103) Minissale, M.; Moudens, A.; Baouche, S.; Chaabouni, H.; Dulieu, F. Hydrogenation of CO-bearing species on grains: unexpected chemical desorption of CO. *Mon. Not. R. Astron. Soc.* **2016**, 458, 2953–2961.

(104) Chuang, K. J.; Fedoseev, G.; Qasim, D.; Ioppolo, S.; van Dishoeck, E. F.; Linnartz, H. Reactive Desorption of CO Hydrogenation Products under Cold Pre-stellar Core Conditions. *Astrophys. J.* **2018**, 853, 102.

(105) Brown, P. D.; Charnley, S. B.; Millar, T. J. A model of the chemistry in hot molecular cores. *Mon. Not. R. Astron. Soc.* **1988**, 231, 409–417.

(106) Bergin, E. A.; Tafalla, M. Cold Dark Clouds: The Initial Conditions for Star Formation. *Annu. Rev. Astron. Astrophys.* **2007**, 45, 339–396.

(107) Garrod, R. T.; Herbst, E. Formation of methyl formate and other organic species in the warm-up phase of hot molecular cores. *Astron. Astrophys.* **2006**, 457, 927–936.

(108) Charnley, S. B.; Tielens, A. G. G. M.; Millar, T. J. On the molecular complexity of the hot cores in Orion A - Grain surface chemistry as 'The last refuge of the scoundrel'. *Astrophys. J.* **1992**, 399, L71–L74.

(109) Rodgers, S. D.; Charnley, S. B. Chemical Evolution in Protostellar Envelopes: Cocoon Chemistry. *Astrophys. J.* **2003**, 585, 355–371.

(110) Aikawa, Y.; Wakelam, V.; Garrod, R. T.; Herbst, E. Molecular Evolution and Star Formation: From Prestellar Cores to Protostellar Cores. *Astrophys. J.* **2008**, 674, 984–996.

(111) Gratier, P.; Majumdar, L.; Ohishi, M.; Roueff, E.; Loison, J. C.; Hickson, K. M.; Wakelam, V. A New Reference Chemical Composition for TMC-1. *Astrophys. J., Suppl. Ser.* **2016**, 225, 25.

(112) Maffucci, D. M.; Wenger, T. V.; Le Gal, R.; Herbst, E. Astrochemical Kinetic Grid Models of Groups of Observed Molecular Abundances: Taurus Molecular Cloud 1 (TMC-1). *Astrophys. J.* **2018**, 868, 41.

(113) Sakai, N.; Yamamoto, S. Warm Carbon-Chain Chemistry. *Chem. Rev.* **2013**, 113, 8981–9015.

(114) Tielens, A. G. G. M.; Hagen, W. Model calculations of the molecular composition of interstellar grain mantles. *Astron. Astrophys.* **1982**, 114, 245–260.

(115) Charnley, S. B.; Rodgers, S. D. Interstellar Reservoirs of Cometary Matter. *Space Sci. Rev.* **2008**, 138, 59–73.

(116) Charnley, S. In *Interstellar Organic Chemistry. The Bridge Between the Big Bang and Biology: Stars, Planetary Systems, Atmospheres, Volcanoes: Their Link to Life*, International workshop, Stromboli, Italy, Sept 13–17, 1999; Giovanelli, F., Ed.; Consiglio Nazionale delle Ricerche: Rome, 2001; p 139.

(117) Hollis, J. M.; Lovas, F. J.; Jewell, P. R. Interstellar Glycolaldehyde: The First Sugar. *Astrophys. J.* **2000**, 540, L107–L110.

(118) Hollis, J. M.; Jewell, P. R.; Lovas, F. J.; Remijan, A. Green Bank Telescope Observations of Interstellar Glycolaldehyde: Low-Temperature Sugar. *Astrophys. J.* **2004**, 613, L45–L48.

(119) Hollis, J. M.; Lovas, F. J.; Jewell, P. R.; Coudert, L. H. Interstellar Antifreeze: Ethylene Glycol. *Astrophys. J.* **2002**, 571, L59–L62.

(120) Hollis, J. M.; Jewell, P. R.; Lovas, F. J.; Remijan, A.; Möllendal, H. Green Bank Telescope Detection of New Interstellar Aldehydes: Propenal and Propanal. *Astrophys. J.* **2004**, 610, L21–L24.

(121) Watanabe, N.; Kouchi, A. Ice surface reactions: A key to chemical evolution in space. *Prog. Surf. Sci.* **2008**, 83, 439–489.

(122) Ioppolo, S.; Cuppen, H. M.; Linnartz, H. Surface formation routes of interstellar molecules: hydrogenation reactions in simple ices. *Rend. Fis. Acc. Lincei* **2011**, 22, 211.

(123) Linnartz, H.; Ioppolo, S.; Fedoseev, G. Atom addition reactions in interstellar ice analogues. *Int. Rev. Phys. Chem.* **2015**, 34, 205–237.

(124) Caselli, P.; Hasegawa, T. I.; Herbst, E. Chemical differentiation between star-forming regions - The Orion Hot Core and Compact Ridge. *Astrophys. J.* **1993**, 408, 548–558.

(125) Rodgers, S. D.; Charnley, S. B. Chemical Differentiation in Regions of Massive Star Formation. *Astrophys. J.* **2001**, 546, 324–329.

(126) Blake, G. A.; Sutton, E. C.; Masson, C. R.; Phillips, T. G. Molecular abundances in OMC-1 - The chemical composition of interstellar molecular clouds and the influence of massive star formation. *Astrophys. J.* **1987**, 315, 621–645.

(127) Charnley, S. B.; Kress, M. E.; Tielens, A. G. G. M.; Millar, T. J. Interstellar Alcohols. *Astrophys. J.* **1995**, 448, 232.

(128) Karpas, Z.; Mautner, M. Alkyl-transfer reactions between protonated alcohols and ethers: gas-phase alkylation of formaldehyde. *J. Phys. Chem.* **1989**, 93, 1859–63.

(129) Cole, C. A.; Wehres, N.; Yang, Z.; Thomsen, D. L.; Snow, T. P.; Bierbaum, V. M. A Gas-phase Formation Route to Interstellar Trans-methyl Formate. *Astrophys. J., Lett.* **2012**, 754, L5.

(130) Neill, J. L.; Steber, A. L.; Muckle, M. T.; Zaleski, D. P.; Lattanzi, V.; Spezzano, S.; McCarthy, M. C.; Remijan, A. J.; Friedel, D. N.; Widicus Weaver, S. L.; Pate, B. H. Spatial Distributions and Interstellar Reaction Processes. *J. Phys. Chem. A* **2011**, 115, 6472–6480.

(131) Neill, J. L.; Muckle, M. T.; Zaleski, D. P.; Steber, A. L.; Pate, B. H.; Lattanzi, V.; Spezzano, S.; McCarthy, M. C.; Remijan, A. J. Laboratory and Tentative Interstellar Detection of Trans-Methyl Formate Using the Publicly Available Green Bank Telescope Primos Survey. *Astrophys. J.* **2012**, 755, 153.

(132) Taquet, V.; Wirstrom, E. S.; Charnley, S. B. Formation and Recondensation of Complex Organic Molecules during Protostellar Luminosity Outbursts. *Astrophys. J.* **2016**, 821, 46.

(133) Laas, J. C.; Garrod, R. T.; Herbst, E.; Widicus Weaver, S. L. Contributions from Grain Surface and Gas Phase Chemistry to the Formation of Methyl Formate and Its Structural Isomers. *Astrophys. J.* **2011**, 728, 71.

(134) Belloche, A.; Garrod, R. T.; Müller, H. S. P.; Menten, K. M.; Comito, C.; Schilke, P. Increased complexity in interstellar chemistry: detection and chemical modeling of ethyl formate and n-propyl cyanide in Sagittarius B2(N). *Astron. Astrophys.* **2009**, 499, 215–232.

(135) Tercero, B.; Cernicharo, J.; López, A.; Brouillet, N.; Kolesnikov, L.; Motiyenko, R. A.; Margulès, L.; Alonso, J. L.; Guillemin, J.-C. Searching for trans ethyl methyl ether in Orion KL. *Astron. Astrophys.* **2015**, 582, L1.

(136) Hamberg, M.; Österdahl, F.; Thomas, R. D.; Zhaunerchyk, V.; Vigren, E.; Kaminska, M.; Af Ugglas, M.; Källberg, A.; Simonsson, A.; Paál, A.; Larsson, M.; Geppert, W. D. Experimental studies of the dissociative recombination processes for the dimethyl ether ions $\text{CD}_3\text{OCD}_2^+$ and $(\text{CD}_3)_2\text{OD}^+$. *Astron. Astrophys.* **2010**, 514, A83.

(137) Boogert, A. C. A.; Gerakines, P. A.; Whittet, D. C. B. Observations of the icy universe. *Annu. Rev. Astron. Astrophys.* **2015**, 53, 541–581.

(138) Skouteris, D.; Balucani, N.; Ceccarelli, C.; Faginas Lago, N.; Codella, C.; Falcinelli, S.; Rosi, M. Interstellar dimethyl ether gas-phase formation: a quantum chemistry and kinetics study. *Mon. Not. R. Astron. Soc.* **2019**, 482, 3567–3575.

(139) Cernicharo, J.; Kisiel, Z.; Tercero, B.; Kolesnikov, L.; Medvedev, I. R.; López, A.; Fortman, S.; Winnewisser, M.; de Lucia, F. C.; Alonso, J. L.; Guillemin, J. C. A rigorous detection of interstellar CH_3NCO : An important missing species in astrochemical networks. *Astron. Astrophys.* **2016**, 587, L4.

(140) Hollis, J. M.; Jewell, P. R.; Remijan, A. J.; Jewell, P. R.; Ilyushin, V. V.; Kleiner, I. Detection of Acetamide (CH_3CONH_2): The Largest Interstellar Molecule with a Peptide Bond. *Astrophys. J.* **2006**, 643, L25–L28.

(141) Shingledecker, C. N.; Tennis, J.; Le Gal, R.; Herbst, E. On Cosmic-Ray-driven Grain Chemistry in Cold Core Models. *Astrophys. J.* **2018**, 861, 20.

(142) Benz, A. O.; et al. Hydrides in young stellar objects: Radiation tracers in a protostar-disk-outflow system. *Astron. Astrophys.* **2010**, 521, L35.

(143) Prasad, S. S.; Tarafdar, S. P. UV radiation field inside dense clouds - Its possible existence and chemical implications. *Astrophys. J.* **1983**, 267, 603–609.

- (144) Bernstein, M. P.; Sandford, S. A.; Allamandola, L. J.; Chang, S.; Scharberg, M. A. Organic Compounds Produced by Photolysis of Realistic Interstellar and Cometary Ice Analogs Containing Methanol. *Astrophys. J.* **1995**, *454*, 327.
- (145) Öberg, K. I.; Garrod, R. T.; van Dishoeck, E. F.; Linnartz, H. Formation rates of complex organics in UV irradiated CH₃OH-rich ices. I. Experiments. *Astron. Astrophys.* **2009**, *504*, 891–913.
- (146) Allen, M.; Robinson, G. W. The molecular composition of dense interstellar clouds. *Astrophys. J.* **1977**, *212*, 396–415.
- (147) D'Hendecourt, L. B.; Allamandola, L. J.; Grim, R. J. A.; Greenberg, J. M. Time-dependent chemistry in dense molecular clouds. II - Ultraviolet photoprocessing and infrared spectroscopy of grain mantles. *Astron. Astrophys.* **1986**, *158*, 119–134.
- (148) Brown, P. D. The grain-surface formation of complex molecules. *Mon. Not. R. Astron. Soc.* **1990**, *243*, 65–71.
- (149) Hollis, J. M.; Vogel, S. N.; Snyder, L. E.; Jewell, P. R.; Lovas, F. J. The Spatial Scale of Glycolaldehyde in the Galactic Center. *Astrophys. J.* **2001**, *554*, L81–L85.
- (150) Sorrell, W. H. Origin of Amino Acids and Organic Sugars in Interstellar Clouds. *Astrophys. J.* **2001**, *555*, L129–L132.
- (151) Viti, S.; Williams, D. A. Time-dependent evaporation of icy mantles in hot cores. *Mon. Not. R. Astron. Soc.* **1999**, *305*, 755–762.
- (152) Garrod, R. T.; Widicus Weaver, S. L.; Herbst, E. Complex Chemistry in Star-forming Regions: An Expanded Gas-Grain Warm-up Chemical Model. *Astrophys. J.* **2008**, *682*, 283–302.
- (153) Ligterink, N. F. W.; Coutens, A.; Kofman, V.; Müller, H. S. P.; Garrod, R. T.; Calcutt, H.; Wampfler, S. F.; Jørgensen, J. K.; Linnartz, H.; van Dishoeck, E. F. The ALMA-PILS survey: detection of CH₃NCO towards the low-mass protostar IRAS 16293–2422 and laboratory constraints on its formation. *Mon. Not. R. Astron. Soc.* **2017**, *469*, 2219–2229.
- (154) Millar, T. J.; Herbst, E. Chemical modelling of dark clouds in the LMC and SMC. *Mon. Not. R. Astron. Soc.* **1990**, *242*, 92–97.
- (155) Acharyya, K.; Herbst, E. Molecular Development in the Large Magellanic Cloud. *Astrophys. J.* **2015**, *812*, 142.
- (156) Acharyya, K.; Herbst, E. Simulations of the Chemistry in the Small Magellanic Cloud. *Astrophys. J.* **2016**, *822*, 105.
- (157) Collings, M. P.; Anderson, M. A.; Chen, R.; Dever, J. W.; Viti, S.; Williams, D. A.; McCoustra, M. R. S. A laboratory survey of the thermal desorption of astrophysically relevant molecules. *Mon. Not. R. Astron. Soc.* **2004**, *354*, 1133–1140.
- (158) Pauly, T.; Garrod, R. T. Modeling CO, CO₂, and H₂O Ice Abundances in the Envelopes of Young Stellar Objects in the Magellanic Clouds. *Astrophys. J.* **2018**, *854*, 13.
- (159) Acharyya, K.; Herbst, E. Hot Cores in Magellanic Clouds. *Astrophys. J.* **2018**, *859*, 51.
- (160) Audard, M.; Abrahám, P.; Dunham, M. M.; Green, J. D.; Grosso, N.; Hamaguchi, K.; Kastner, J. H.; Kóspál, Á.; Lodato, G.; Romanova, M. M.; Skinner, S. L.; Vorobyov, E. I.; Zhu, Z. Episodic Accretion in Young Stars. *Protostars and Planets VI* **2014**, 387–410.
- (161) Buckle, J. V.; Rodgers, S. D.; Wirstrom, E. S.; Charnley, S. B.; Markwick-Kemper, A. J.; Butner, H. M.; Takakuwa, S. Observations of chemical differentiation in clumpy molecular clouds. *Faraday Discuss.* **2006**, *133*, 63–82.
- (162) Wirstrom, E. S.; Charnley, S. B.; Persson, C. M.; Buckle, J. V.; Cordiner, M. A.; Takakuwa, S. Cold Water Vapor in the Barnard 5 Molecular Cloud. *Astrophys. J., Lett.* **2014**, *788*, L32.
- (163) Mumma, M. J.; Charnley, S. B. The Chemical Composition of Comets - Emerging Taxonomies and Natal Heritage. *Annu. Rev. Astron. Astrophys.* **2011**, *49*, 471–524.
- (164) Oliveira, J. M. The star formation process in the Magellanic Clouds. *The Magellanic System: Stars, Gas, and Galaxies*, Symposium 256; van Loon, J. T., Oliveira, J. M., Eds.; International Astronomical Union, 2009; pp 191–202.
- (165) Fedoseev, G.; Chuang, K.-J.; Ioppolo, S.; Qasim, D.; van Dishoeck, E. F.; Linnartz, H. Formation of Glycerol through Hydrogenation of CO Ice under Prestellar Core Conditions. *Astrophys. J.* **2017**, *842*, 52.